

Coastal Dynamical Processes

We introduce the basic notions relative to different aspects, both theoretical and practical, of the study of coastal dynamical processes.

We have dealt with geological issues, physical and mathematical modelling, effects related to human activities, Geographical Information Systems.

It is important to define well the Integrated Management of Coastal Zone (gestione integrata delle zone costiere - GIZC), to improve a sustainable approach to reduce the negative effect as consequence to erosion and climate change on coastal environment/habitat.

Coastal Dynamics

Judith Bosboom and Marcel J.F. Stive

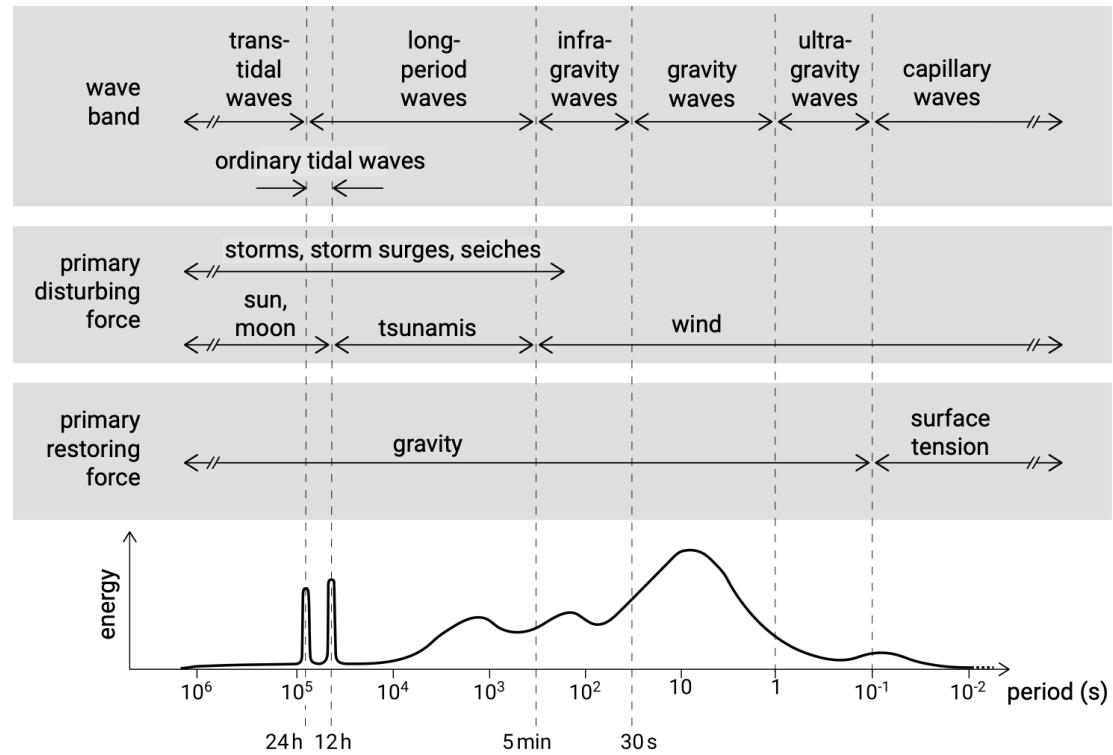


Figure 3.2: Sketch of the relative amounts of energy as a function of wave period in ocean waves. The top section gives the classification based on wavelength, the section below the classification based on the wave-generating force, and the bottom section the classification based on the restoring force. After Munk (1950) and Kinsman (1965).

Table 1-1. Grain size model of American Geophysical Union (van Rijn, 1993)

Class Name	Millimeters	Micrometers	Phi Values
Boulders	>256		<-8
Cobbles	256-64		-8 to -6
Gravel	64-2		-6 to -1
Very coarse sand	2.0-1.0	2000-1000	-1 ~ 0
Coarse sand	1.0-0.5	1000-500	0 ~ +1
Medium sand	0.5-0.25	500-250	+1 ~ +2
Fine sand	0.25-0.125	250-125	+2 ~ +3
Very fine sand	0.125-0.062	125-62	+3 ~ +4
Coarse silt	0.062-0.031	62-31	+4 ~ +5
Medium silt	0.031-0.016	31-16	+5 ~ +6
Fine silt	0.016-0.008	16-8	+6 ~ +7
Very fine silt	0.008-0.004	8-4	+7 ~ +8
Coarse clay	0.004-0.002	4-2	+8 ~ +9
Medium clay	0.002-0.001	2-1	+9 ~ +10
Fine clay	0.001-0.0005	1-0.5	+10 ~ +11
Very fine clay	0.0005-0.00024	0.5-0.25	+11 ~ +12
Colloids	<0.00024	<0.024	>+12

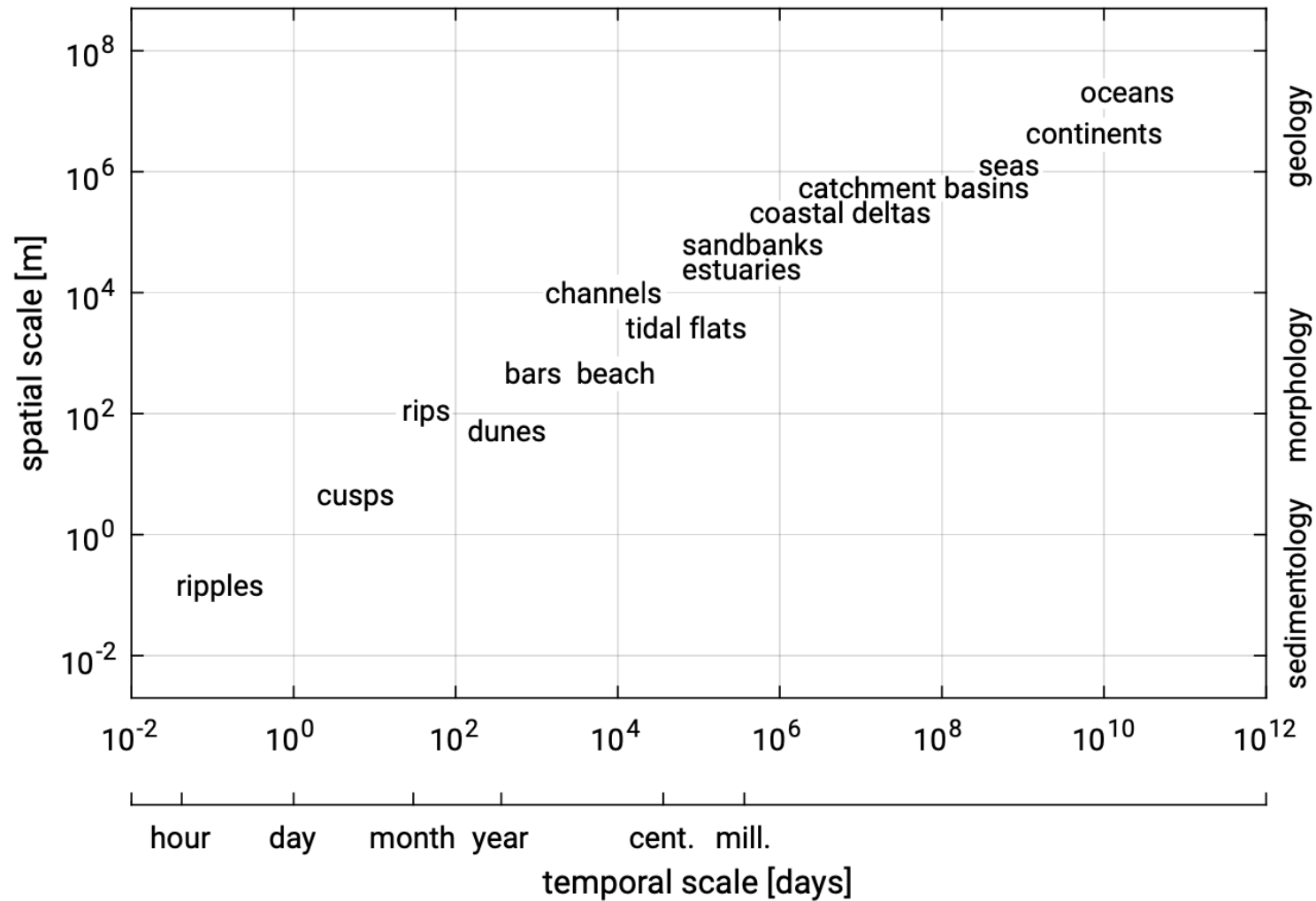


Figure 1.17: Coastal phenomena span a large range of time- and spatial scales, with time- and spatial scales being closely related. For this figure, we followed the categorisation of coastal phenomena by Dronkers (2005).

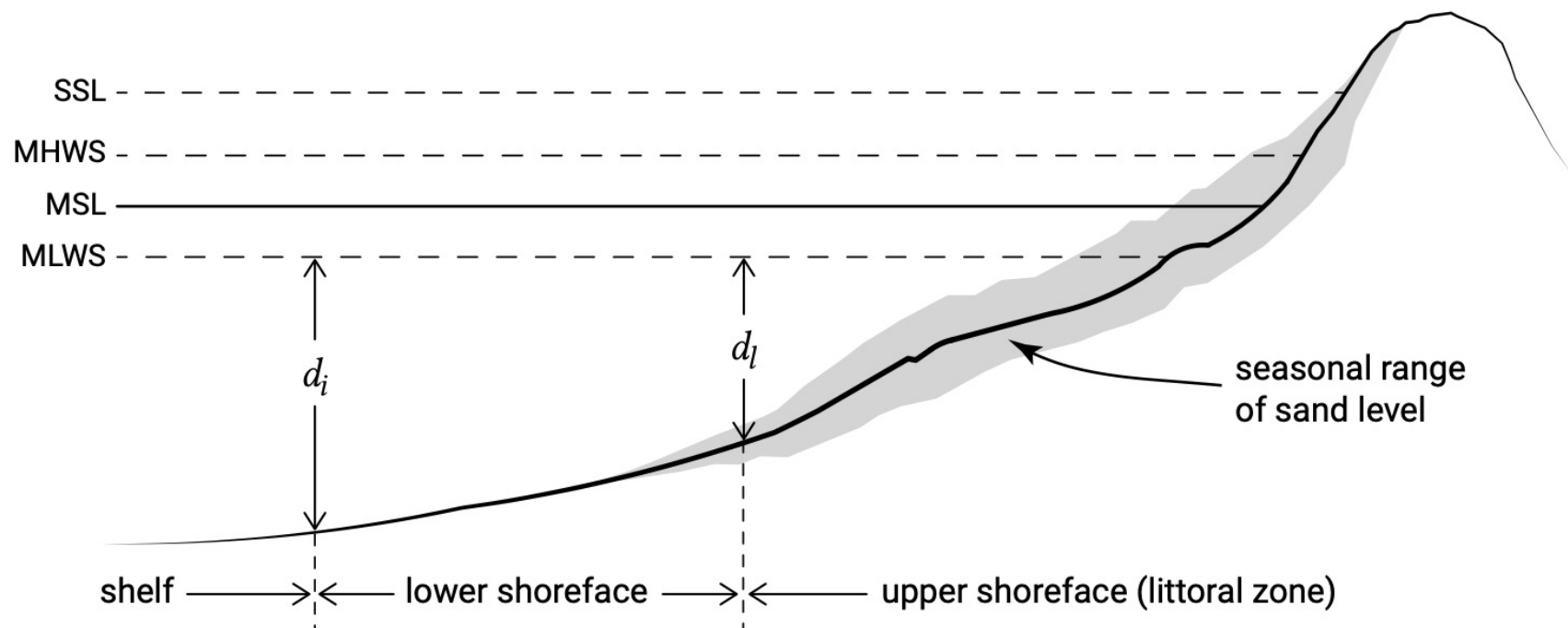


Figure 1.14: Envelope of beach profiles measured at different times, over a period of for instance a year. The two depth limits d_i and d_l correspond to the closure depth definition of Hallermeier (1978, 1981), see also Sect. 7.2.3. The profile is dynamic landward of the outer depth limit d_l . The majority of the bed dynamics takes place at depths smaller than the inner depth limit or annual closure depth d_l , where d_l is the maximum water depth for nearshore erosion by extreme conditions exceeded for twelve hours per year. The tidal levels Mean High Water Spring (MHWS) and Mean Low Water Spring (MLWS) are explained in App. C.

Krumbein phi scale

Size ranges define limits of classes that are given names in the Wentworth scale (or Udden–Wentworth scale) used in the [United States](#). The Krumbein *phi* (ϕ) scale, a modification of the Wentworth scale created by [W. C. Krumbein^{\[1\]}](#) in 1934, is a [logarithmic scale](#) computed by the equation

$$\Phi = -\log_2 (D/D_0)$$

where

Φ is the Krumbein phi scale

D is the [diameter](#) of the particle or grain in millimeters (Krumbein and Monk's equation) and

D_0 is a reference diameter, equal to 1 mm (to make the equation [dimensionally consistent](#)).

This equation can be rearranged to find diameter using ϕ

$$D = D_0 * \Phi^{-2}$$

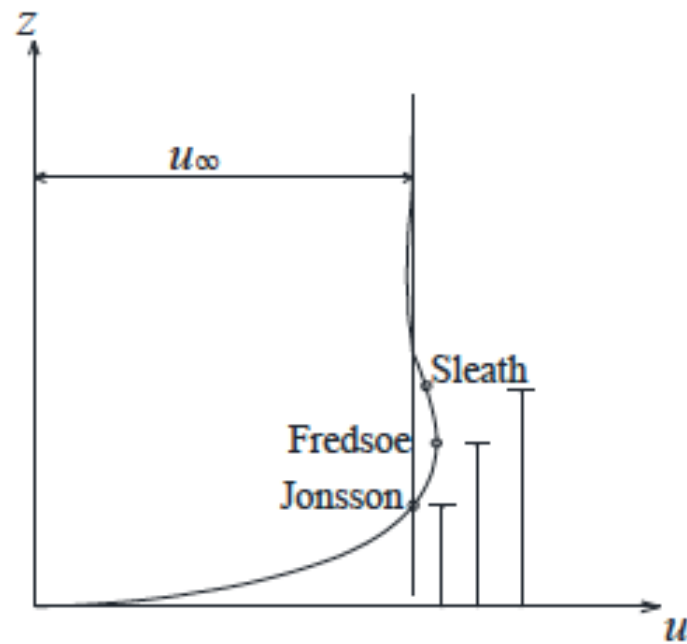


Figure 1-4. Sketch of velocity distribution in wave bottom boundary layer (after Jonsson (1966) and You (1994))

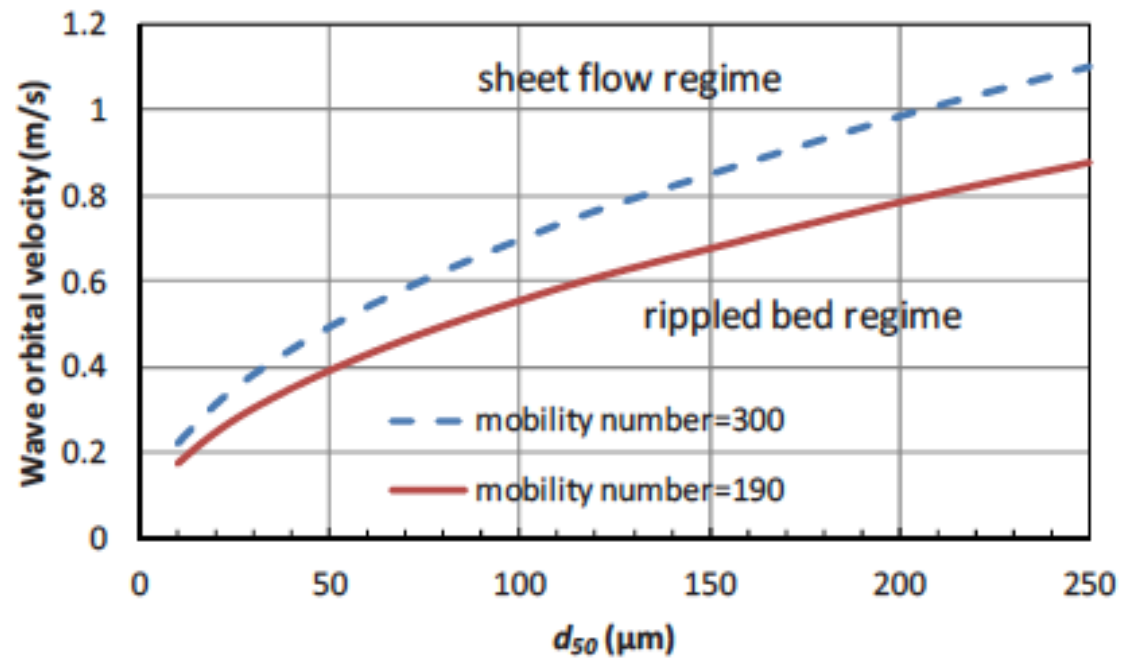
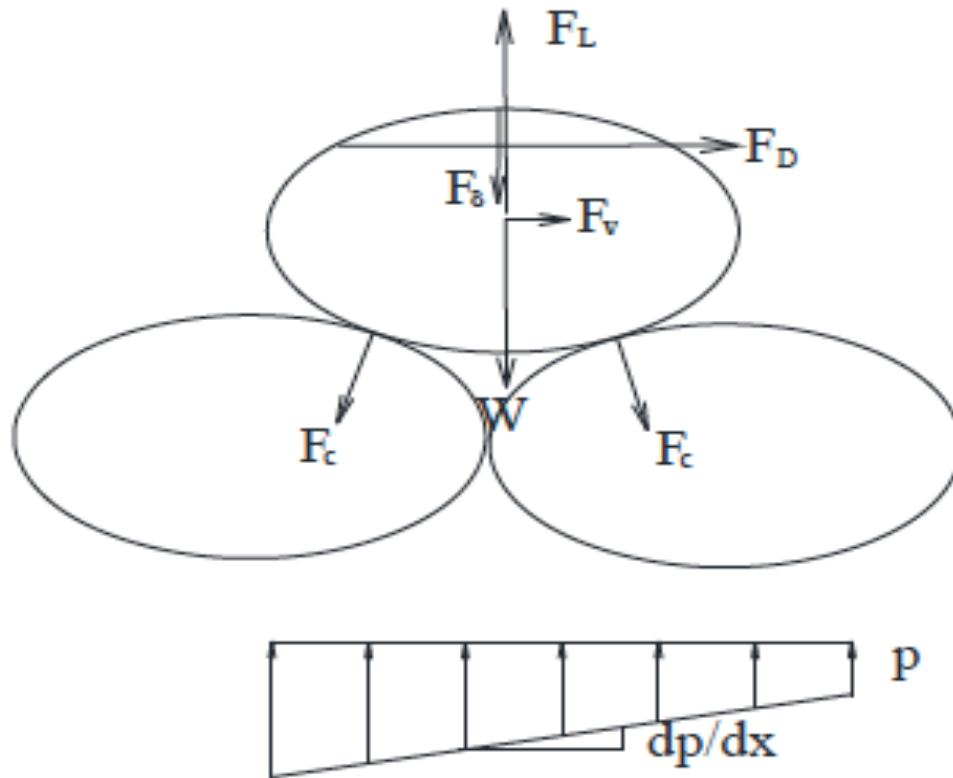


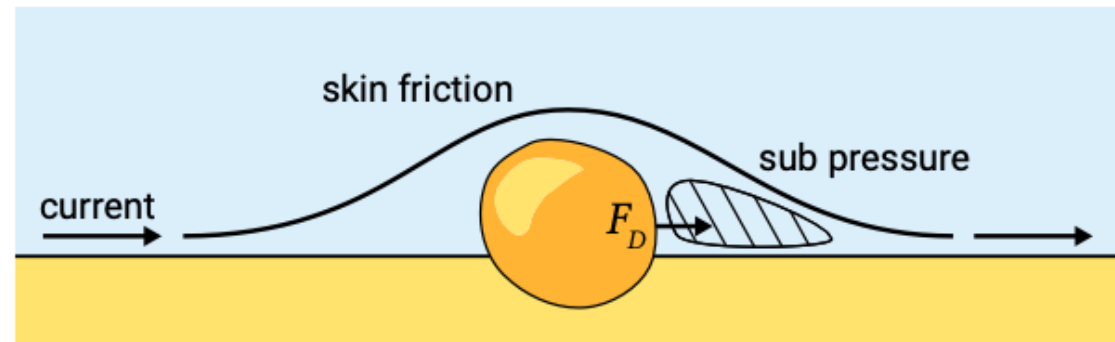
Figure 1-6. The criterion conditions of bed forms according to O'Donoghue et al. (2006)



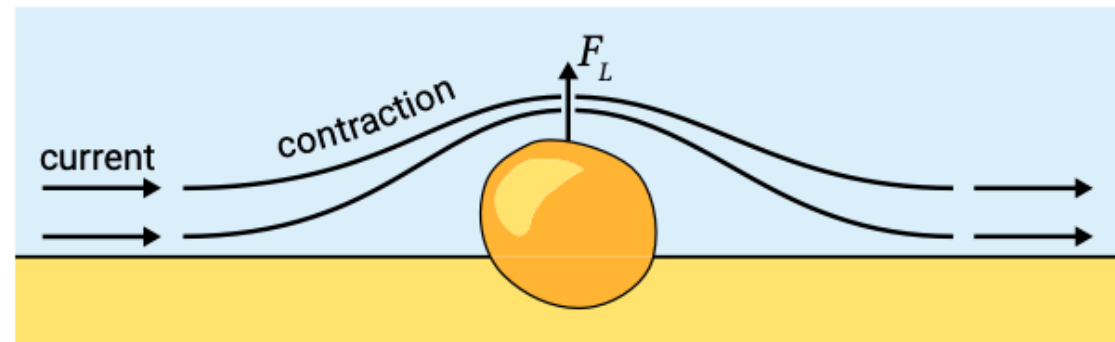
F_L Lift force
 F_δ static water pressure
 F_v wave-inertia force
 F_c cohesive force
 F_D Drag force
 W gravity

Figure 3-1. Forces acting on a single particle

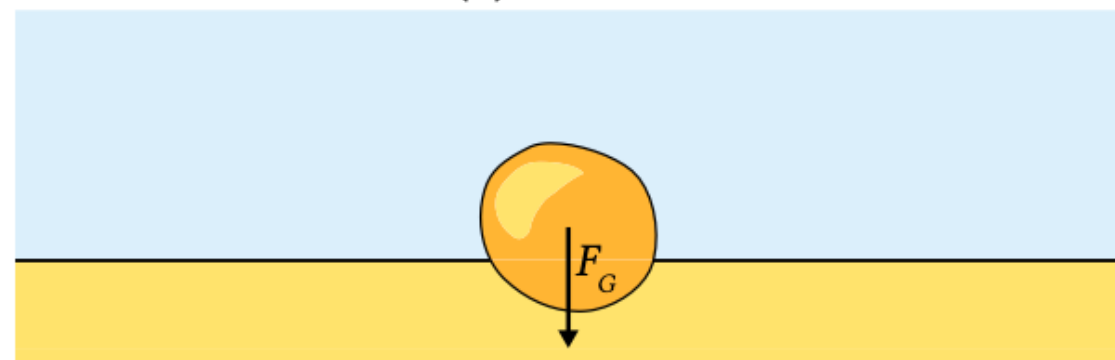
Source: https://www.un-ihe.org/sites/default/files2018_ihe_phd_thesis_zuo_i.pdf



(a) drag force (in the direction of the current)



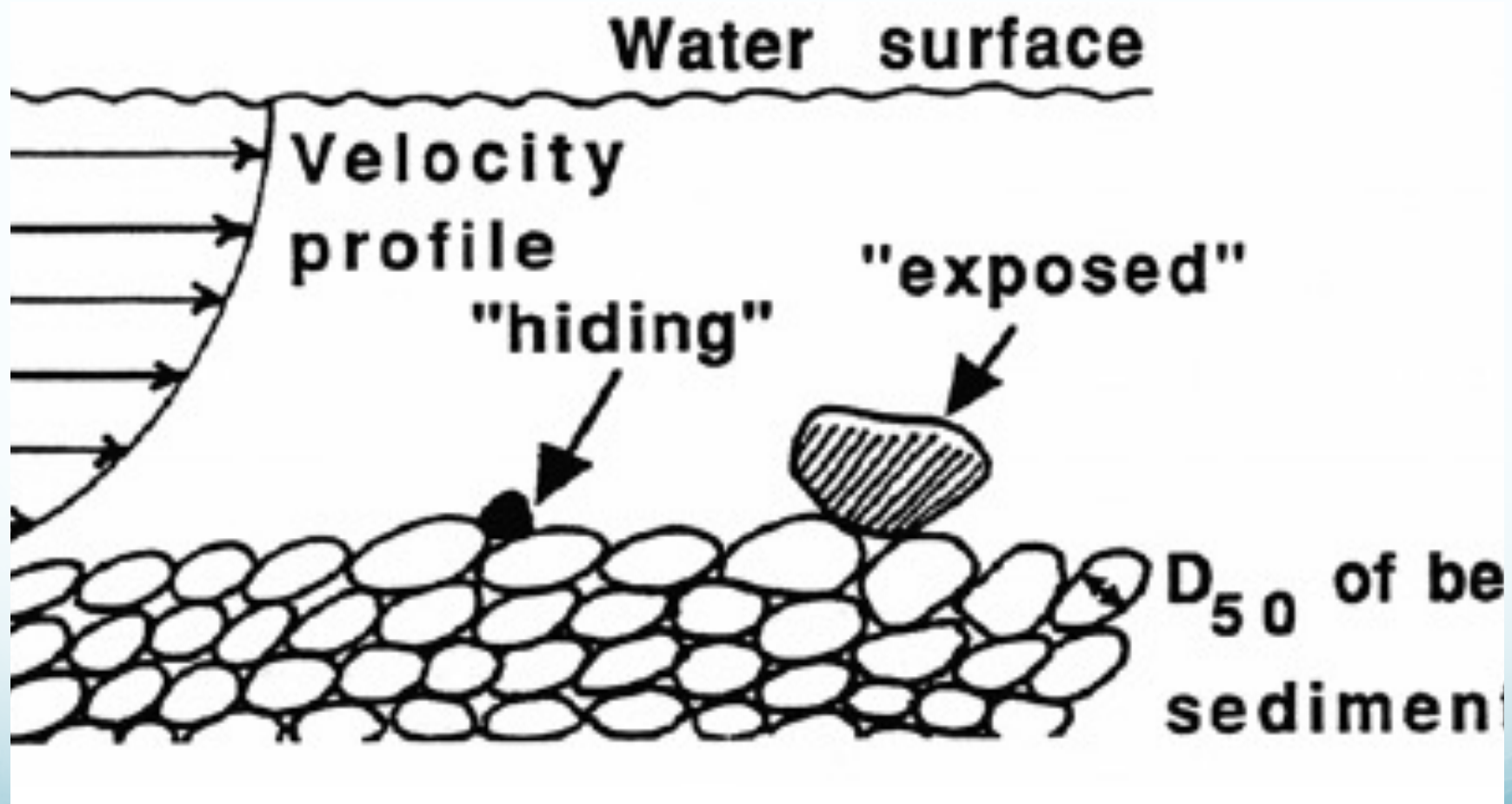
(b) lift force



(c) gravity force

Figure 6.4: Forces on an individual grain in a stationary situation.





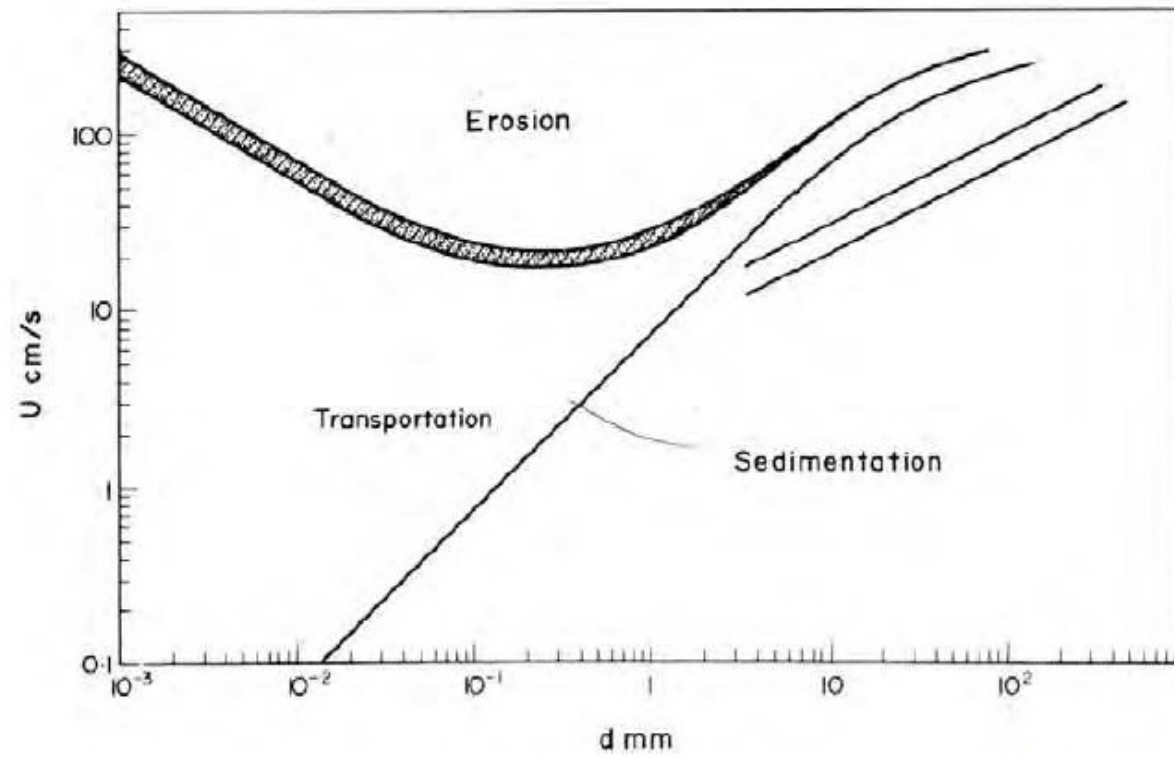
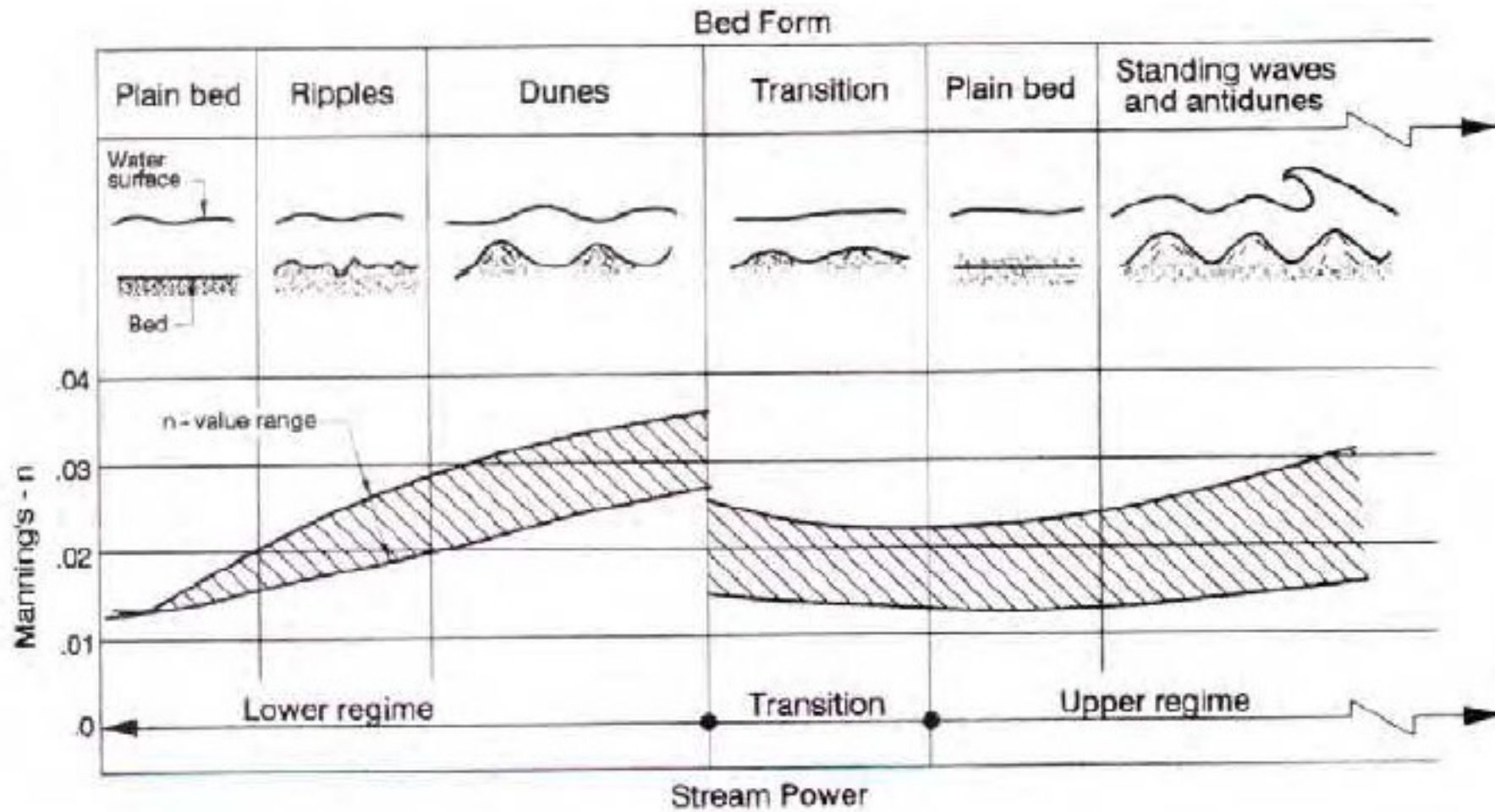
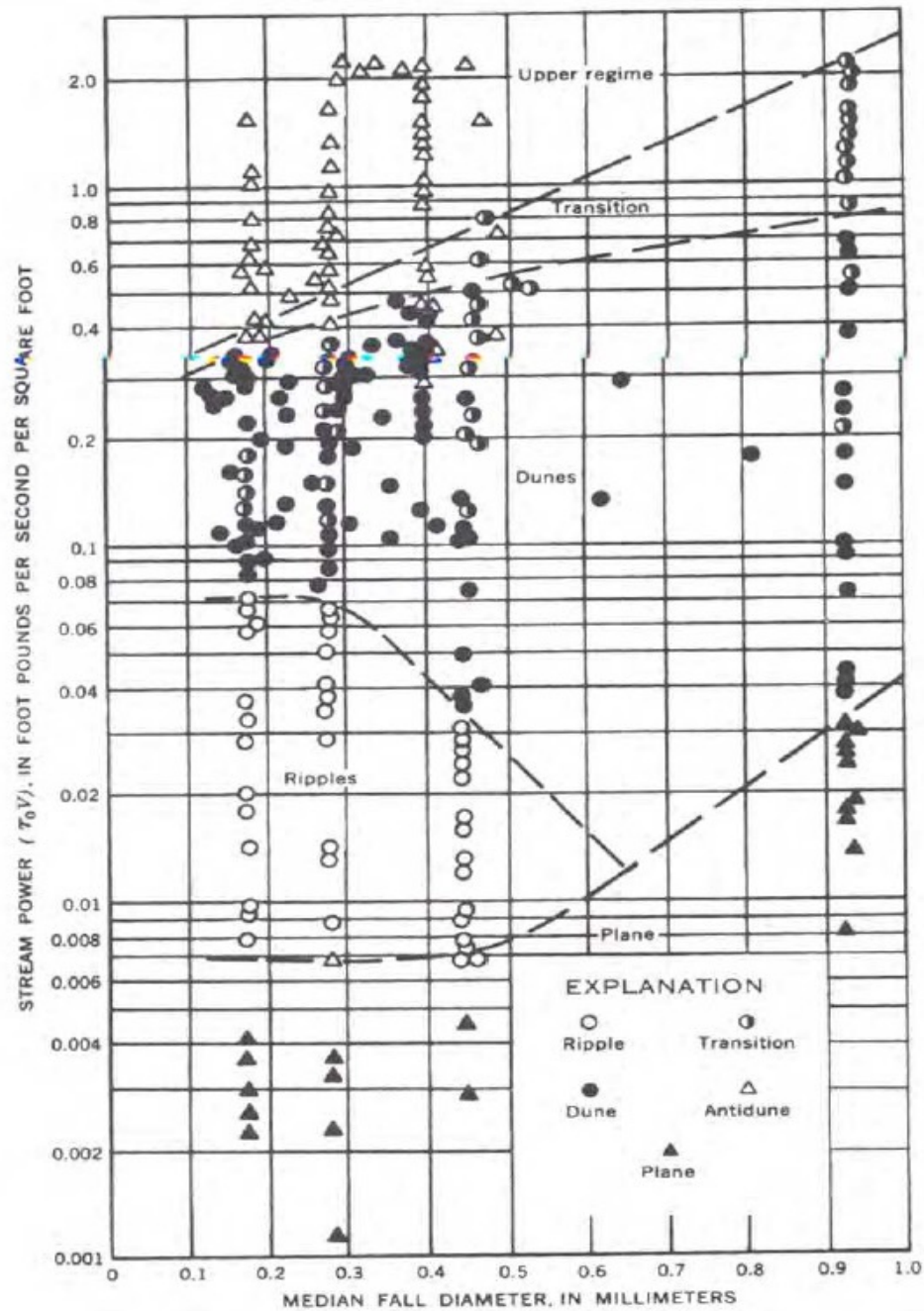


Fig. 1.3. Erosion and deposition criteria for uniform particles (Hjulström, 1935)

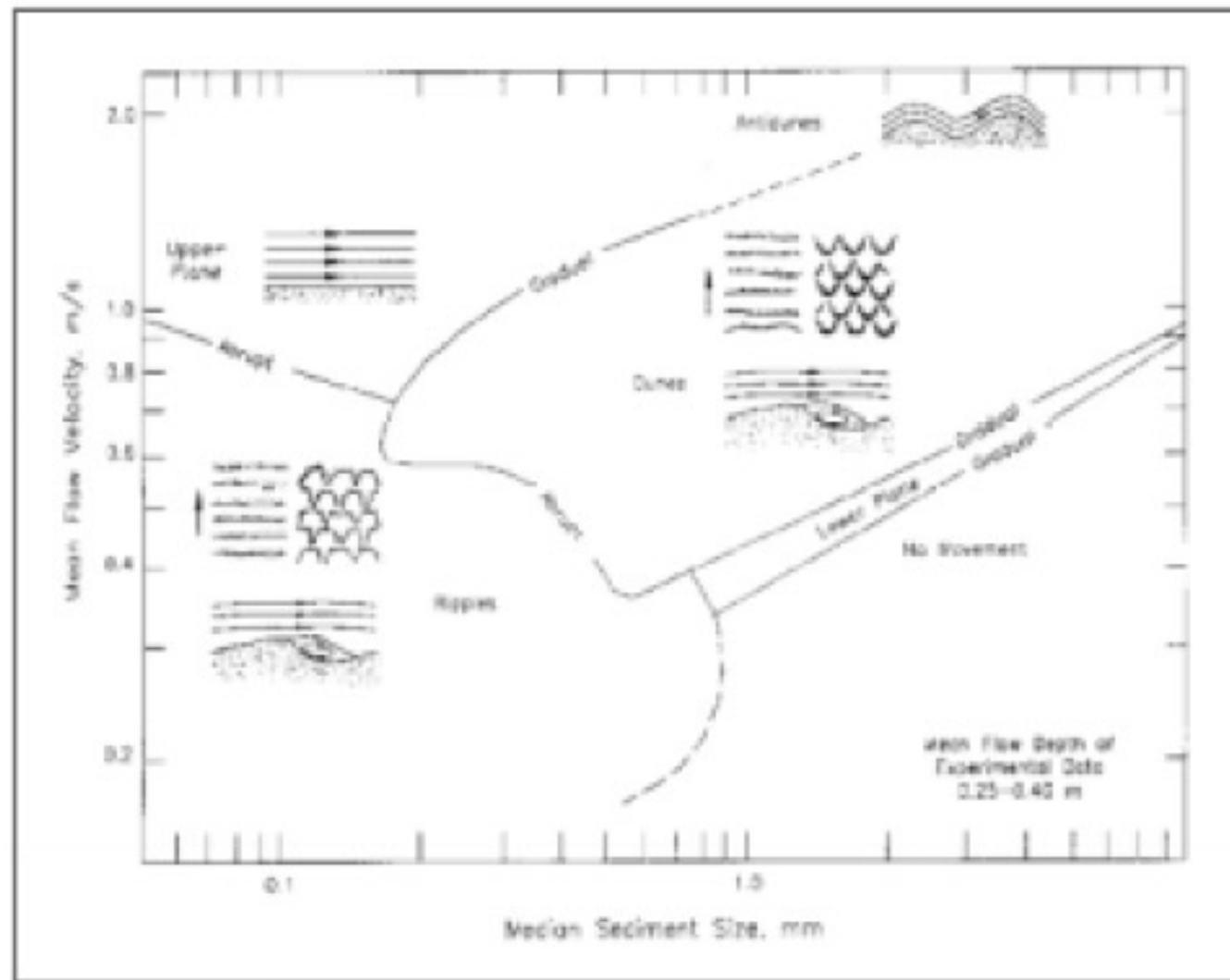


Source: www.intechopen.com

Source: www.intechopen.com



Predictional bed form type based on stream power (Simons and Richardson, 1966)



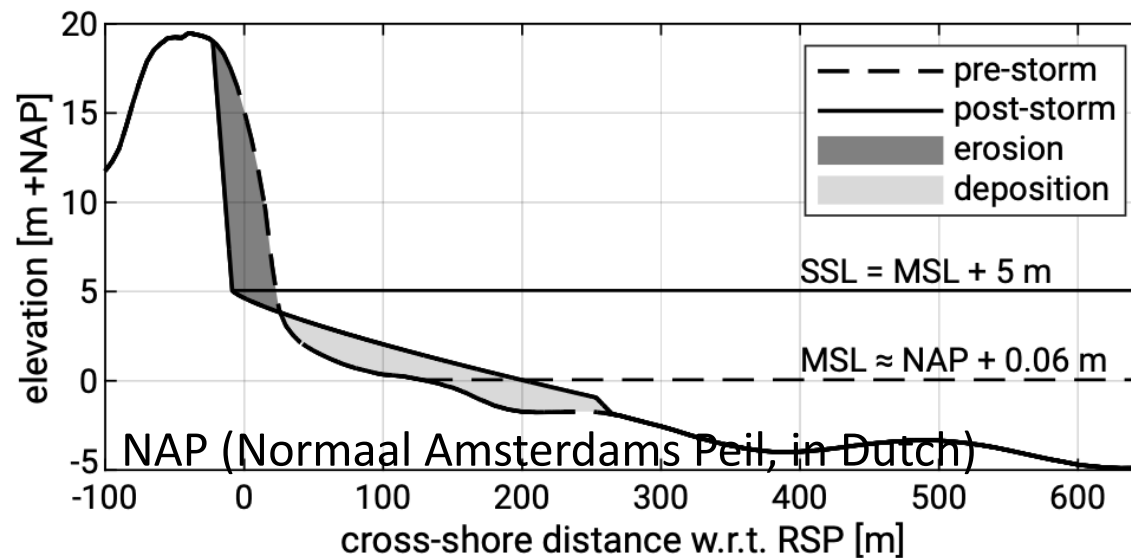


Figure 1.13: Illustration of a storm impact on the cross-shore profile. The pre-storm profile (dashed line) is a typical summer profile (summer 2015) for the Dutch coast, averaged over a 3 km long stretch near Zandvoort (data from JARKUS, [n.d.](#)). The post-storm profile (solid black line) as a consequence of a storm surge with Storm Surge Level (SSL) and storm wave conditions is estimated after (Vellinga, 1986), see Fig. 7.18 for details.

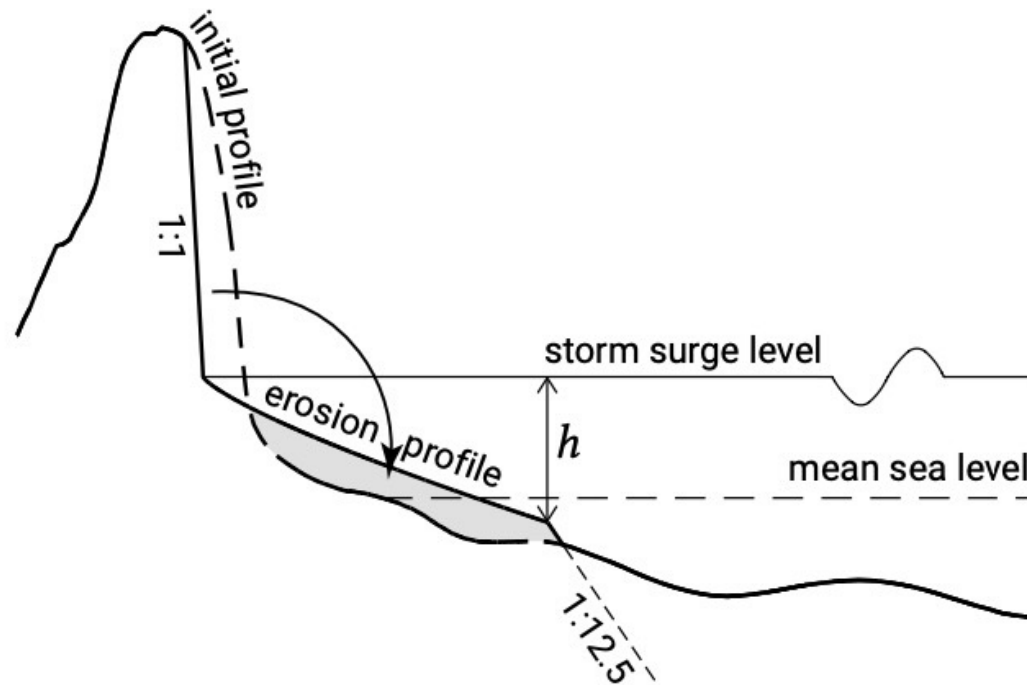
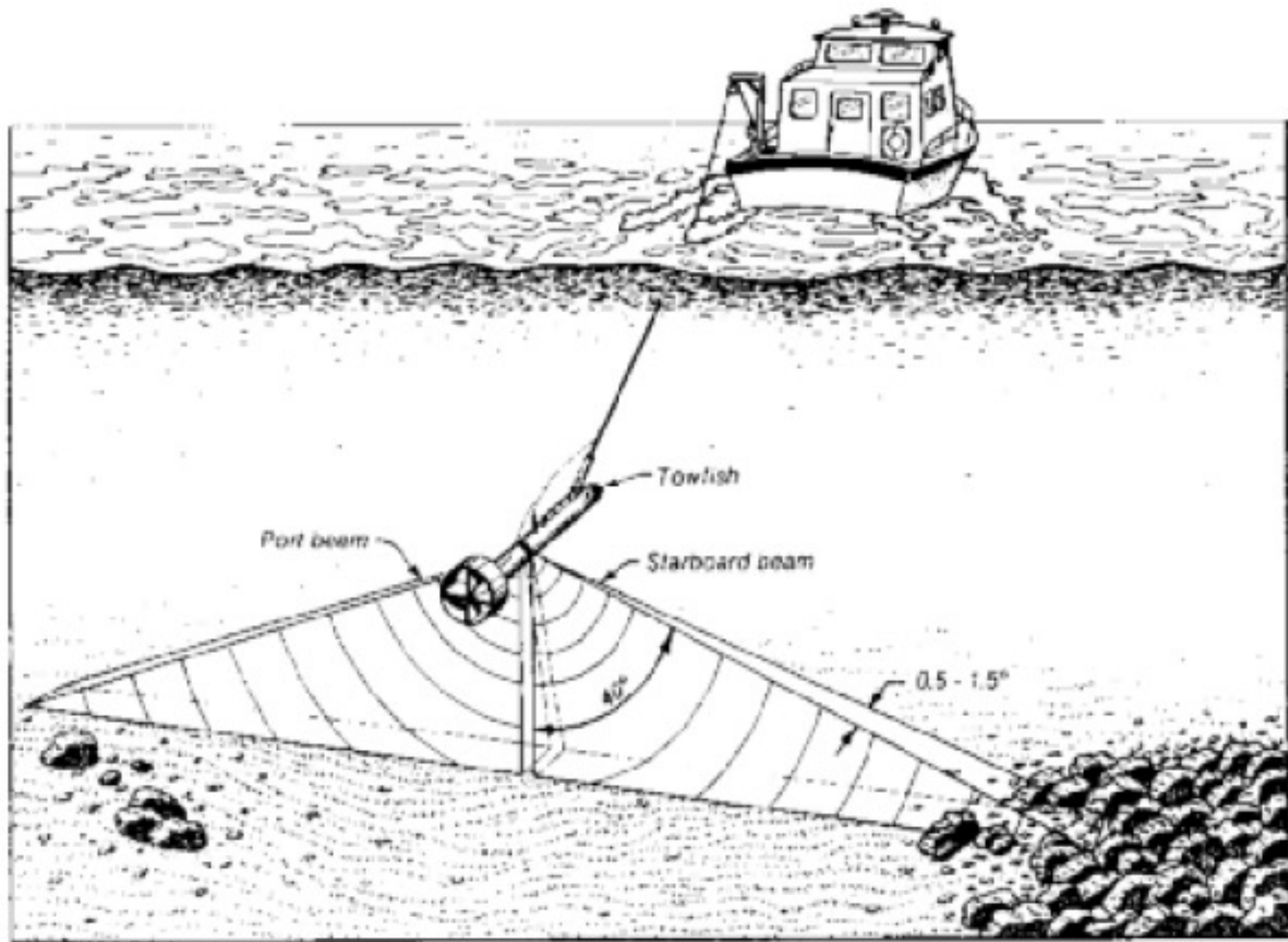


Figure 7.18: Extent of the sedimentation zone to a depth h equal to approximately 75% of the offshore (significant) wave height $H_s = 8$ m. The 'erosion profile' or post-storm profile (after Vellinga, 1986) has a prescribed shape (Eq. 7.10 with $A = 0.078$) and its location is determined by balancing the volumes of erosion (higher in the profile) and accretion (lower in the profile). The vertical and horizontal scale are not the same (the 1:1 slope is a 45° slope in reality). The initial profile matches Fig. 1.13 and $SSL = 5$ m.



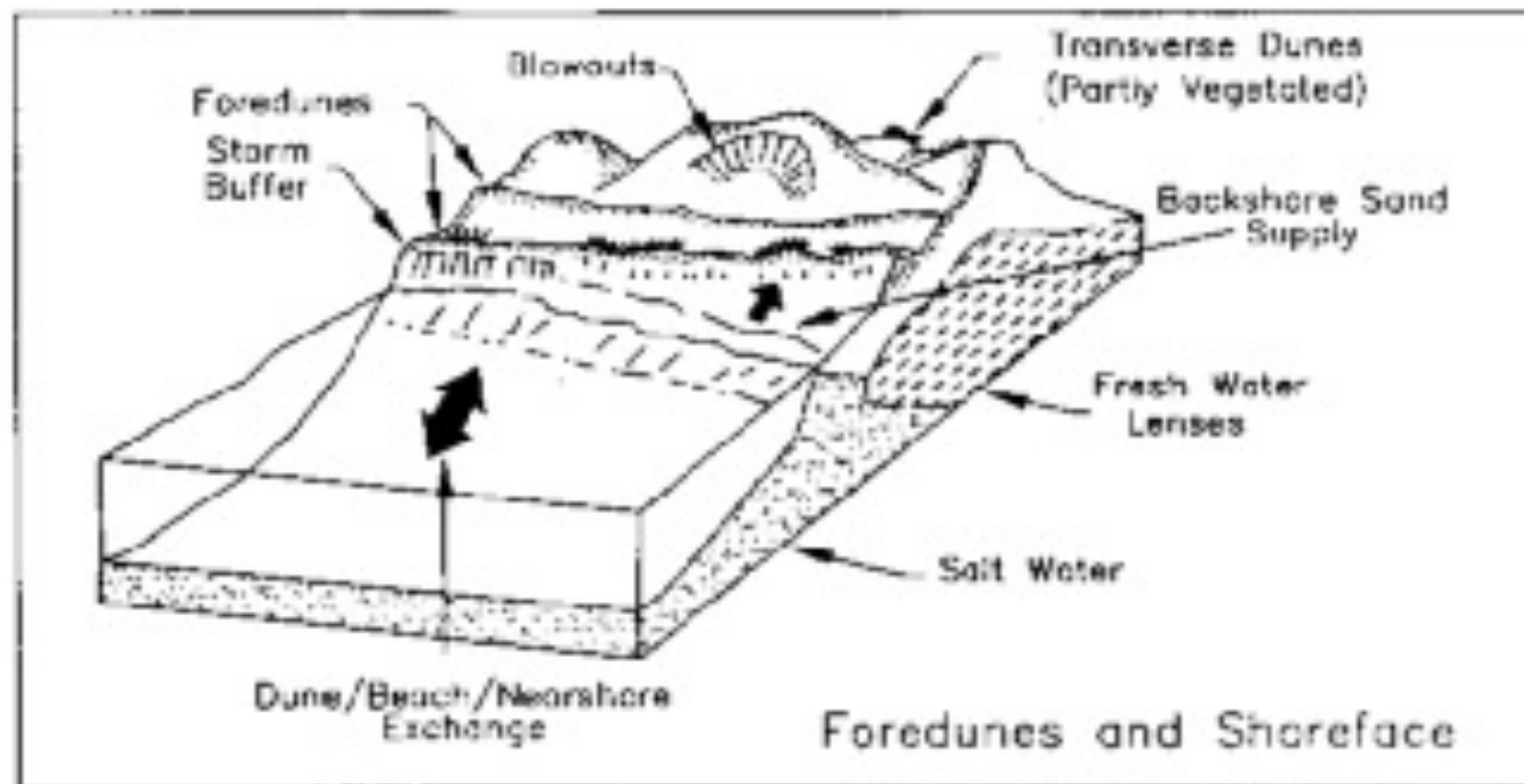
Definitions:

1 Ripples. Little bottom shape characterized by a distance between them less than 0,6 m and height less than 0,03 m.

2 Dunes. Similar for the morphological shape at ripples, but characterized by dimension ranging from 1 to 1.000 meters
They are realized in presence of unidirectional current in water with depth greater than 1 meter and dimension of sediments greater than 0,15 mm and value of the velocity of current greater then 0,4 m/s.

3 Flat bottom when depression or step are not present.

COASTAL DUNES



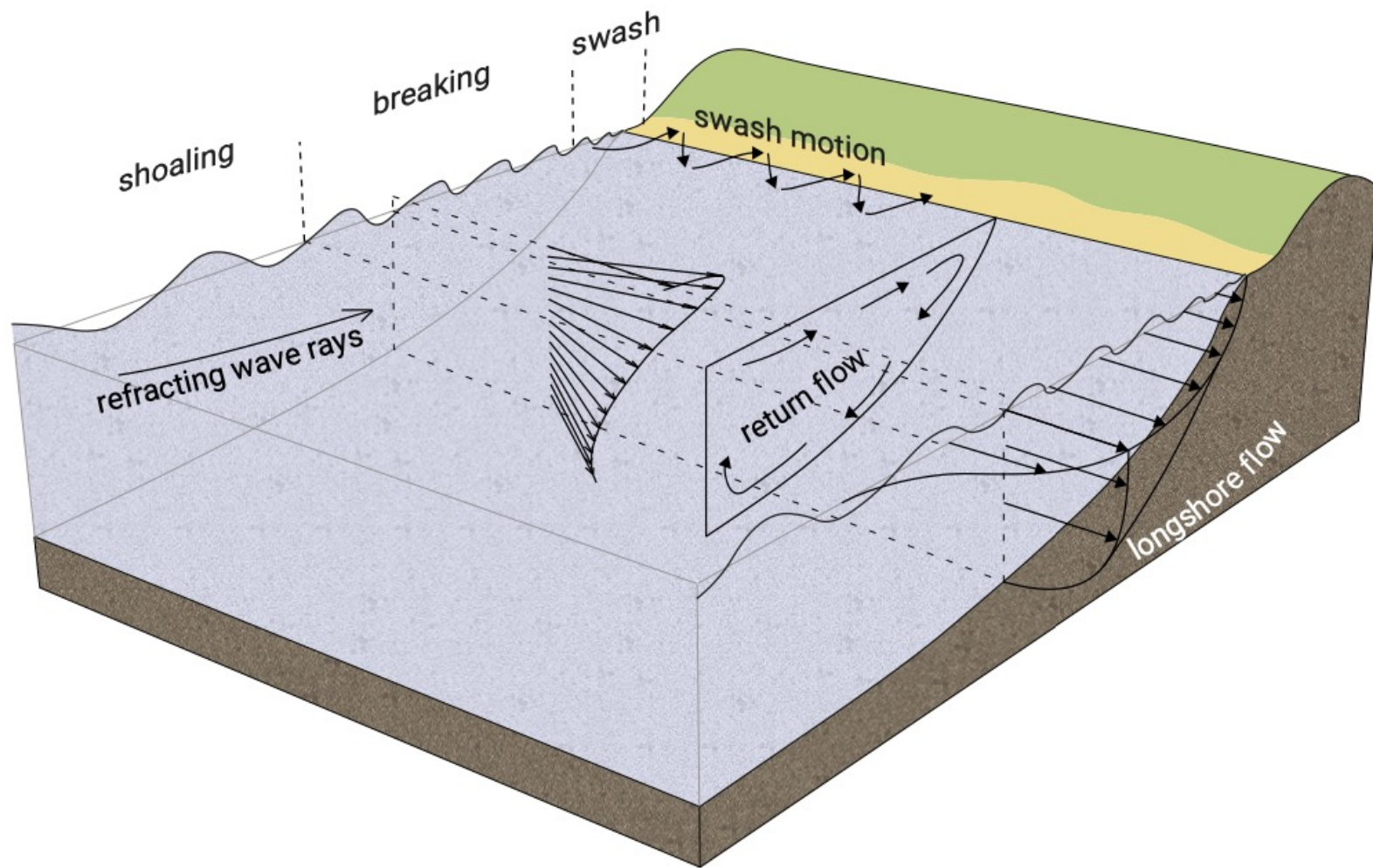
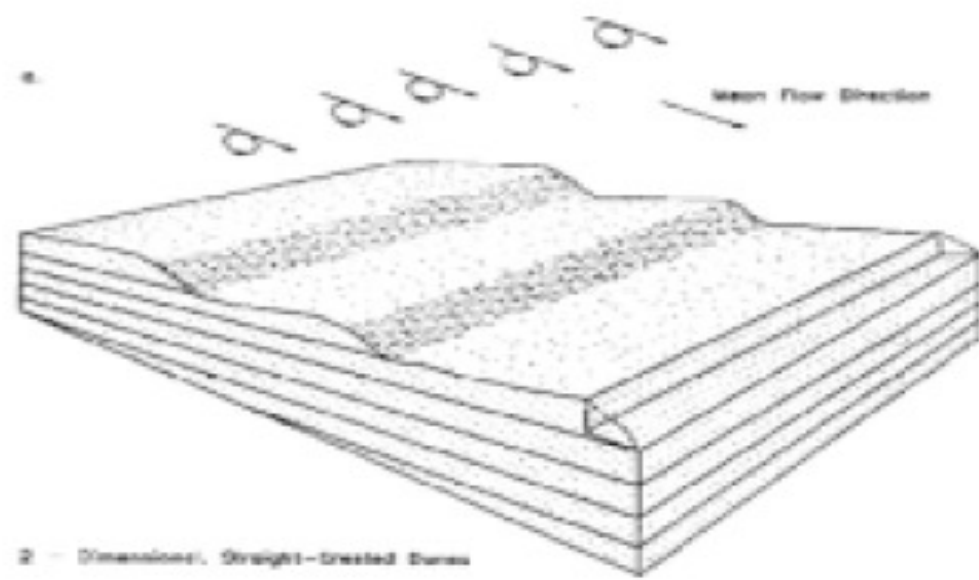
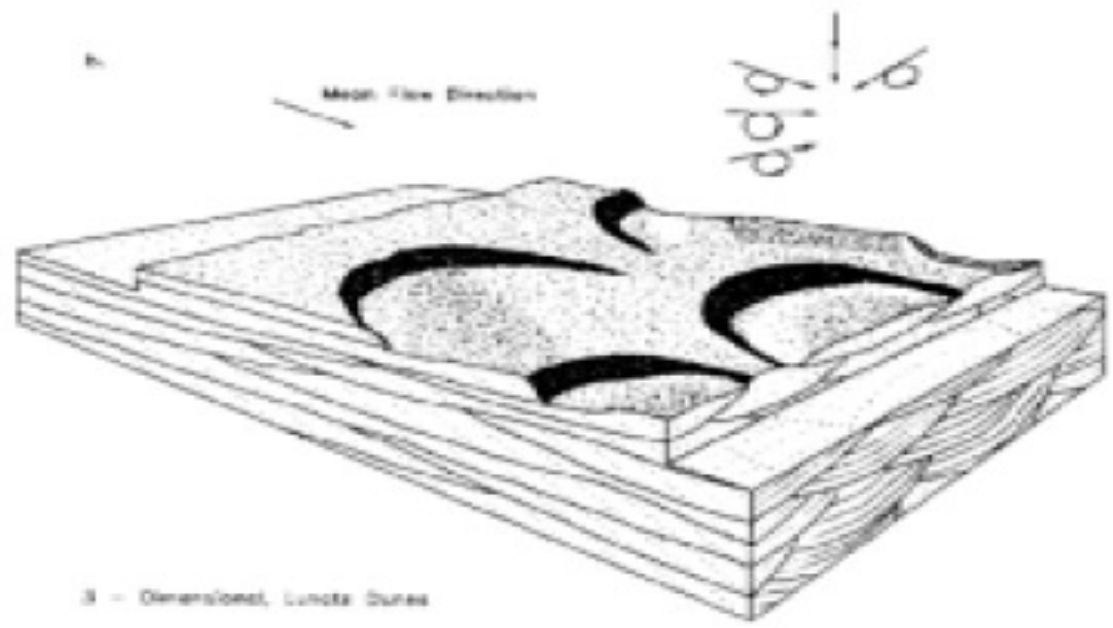


Figure 5.44: 3D structure of the wave-induced current profile in the surf zone, composed of the undertow and the alongshore current.



2 - Dimensional, Straight-Crested Dunes



3 - Dimensional, Lunette Dunes

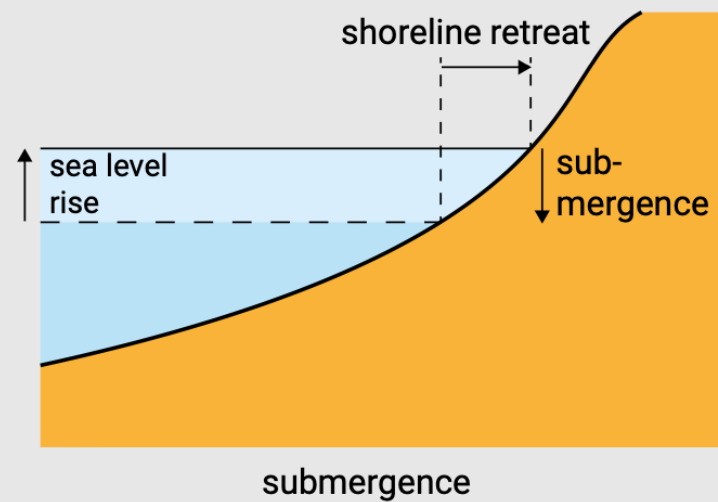
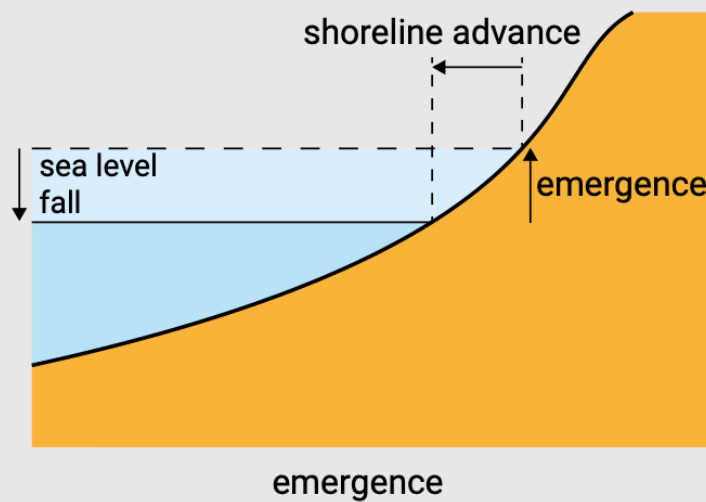
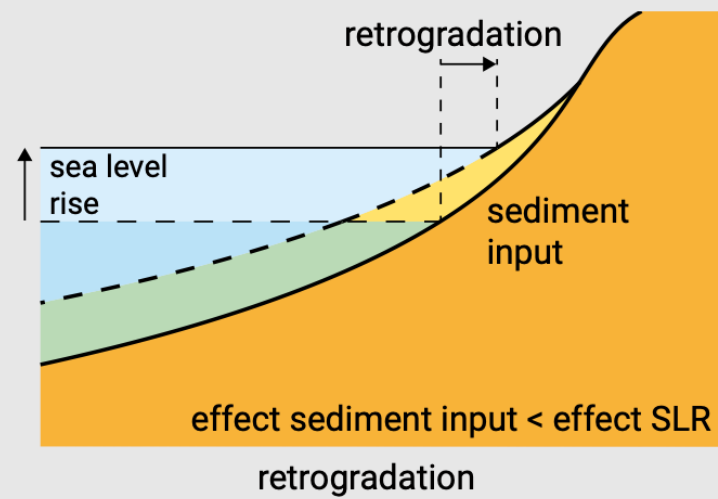
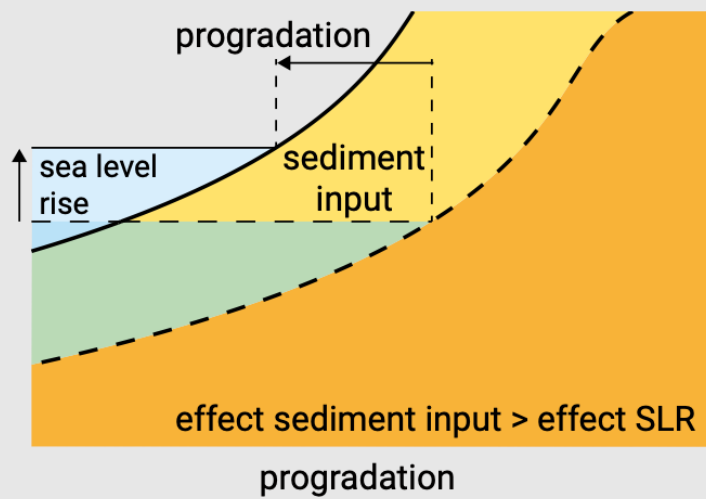


Figure 2.24: Classifications on the basis of sea level change and sediment supply. In the case of sea level rise, the occurrence of progradation or retrogradation depends on the amount of sediment input or loss. Note that the shoreline response in the sketches for emergence and submergence does not take the Bruun effect into account (see Fig. 2.22).

Conservation of soil and water requires both knowledge of the factors affecting these resources, and methods for controlling those factors to preserve those resources.

Soil erosion is a major problem around the world because of its effects on soil productivity, nutrient loss, siltation in water bodies, and degradation of water quality. By understanding the **driving forces** behind soil erosion, it is necessary to identify erosion-prone areas within a landscape and use land management and other strategies to effectively manage the problem.

Soil erosion models have been used to assist in this task. One of the most commonly used soil erosion models is the Universal Soil Loss Equation (USLE) and its family of models: Revised as RUSLE, RUSLE2, and the Modified as MUSLE.

The USLE soil loss equation is:

$$A = R K L S C P$$

where

A Mean annual soil loss (metric tons hectare⁻¹ year⁻¹)

R Rainfall and runoff factor or rainfall erosivity factor (megajoules millimetre hectare⁻¹ hour⁻¹ year⁻¹)

K Soil erodibility factor (metric tons hectare hour megajoules⁻¹ hectare⁻¹ millimetre⁻¹)

L Slope-length factor (unitless)

S Slope-steepness factor (unitless)

C Cover and management factor (unitless)

P Support practice factor (unitless)

A method of determining the C-factor is through the Normalized Difference Vegetation Index (NDVI) that estimated from satellite imagery.

RUSLE Soil loss estimation

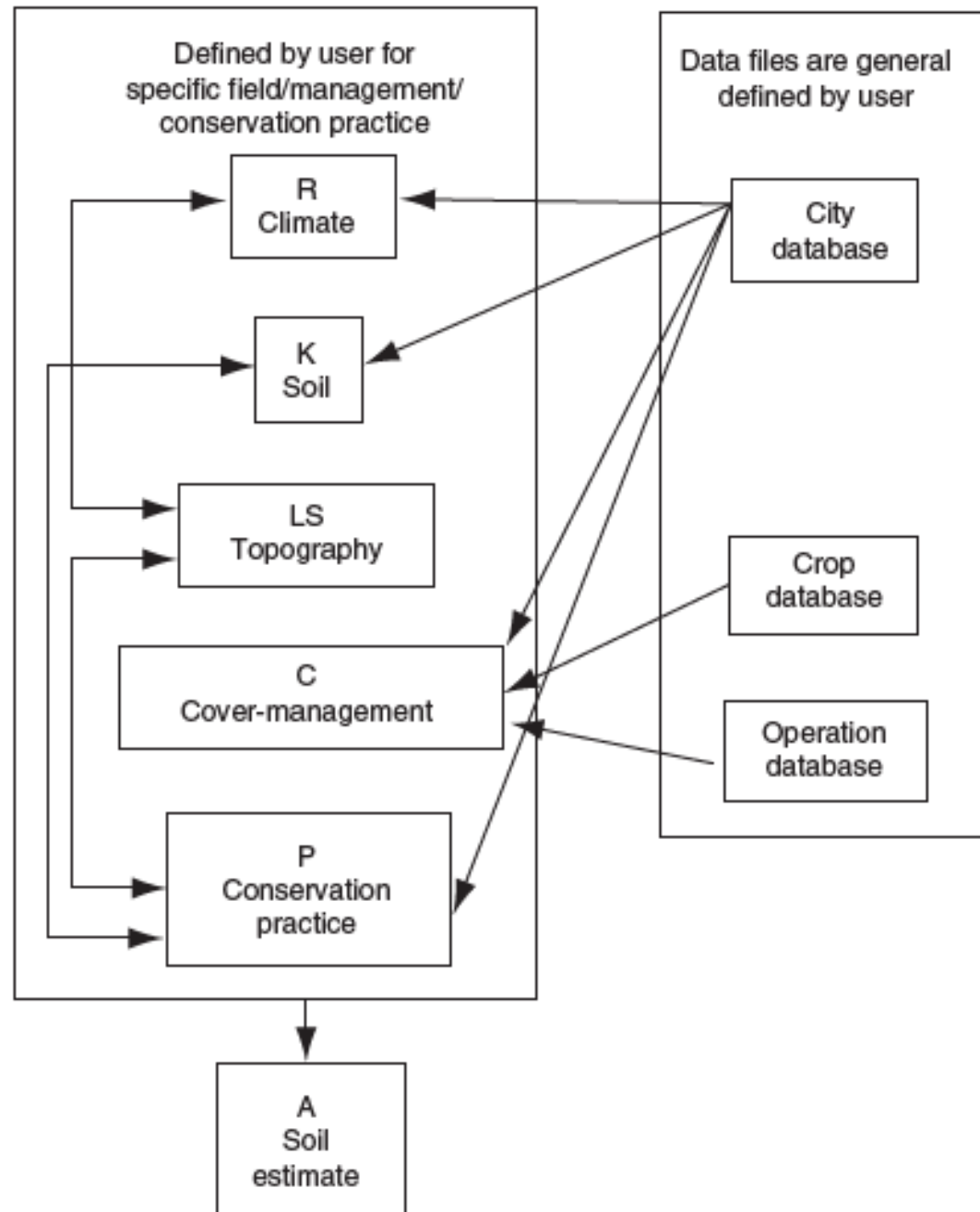
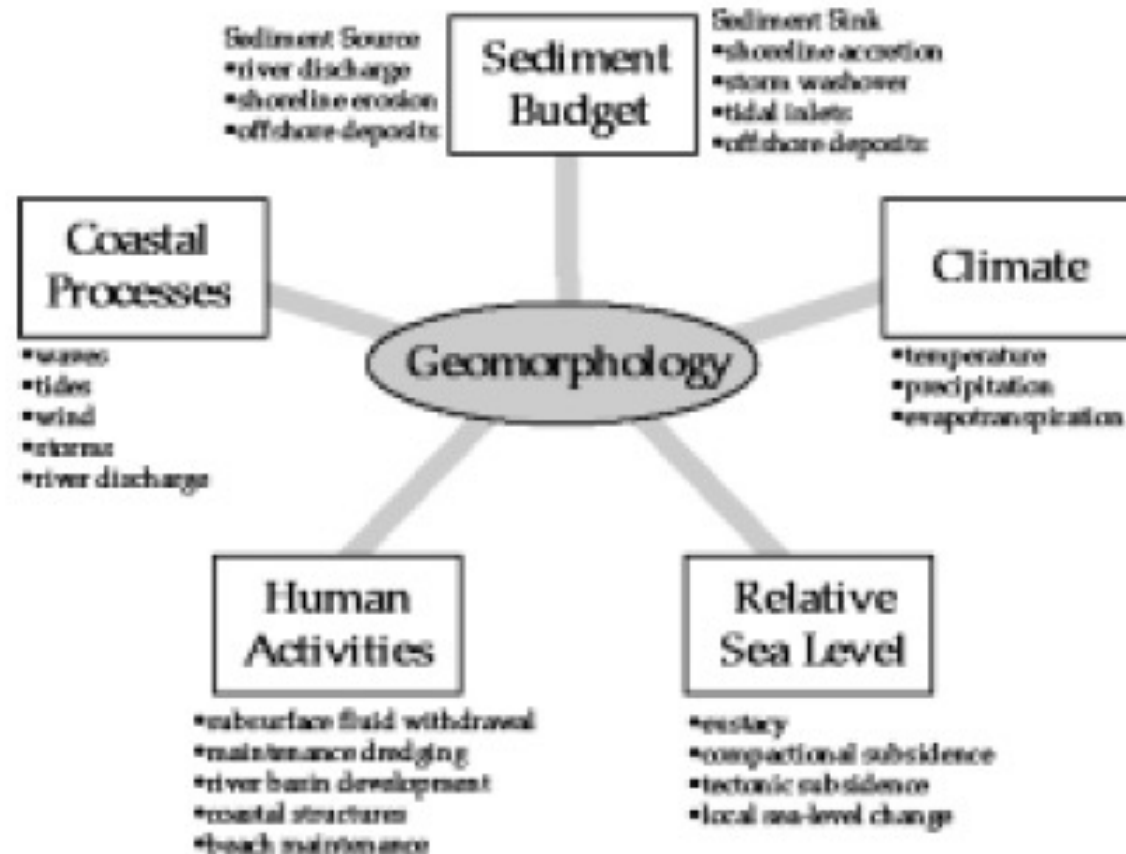


Fig. 8.1 RUSLE1 software flow chart (from AH703).

Shoreline Change Variables



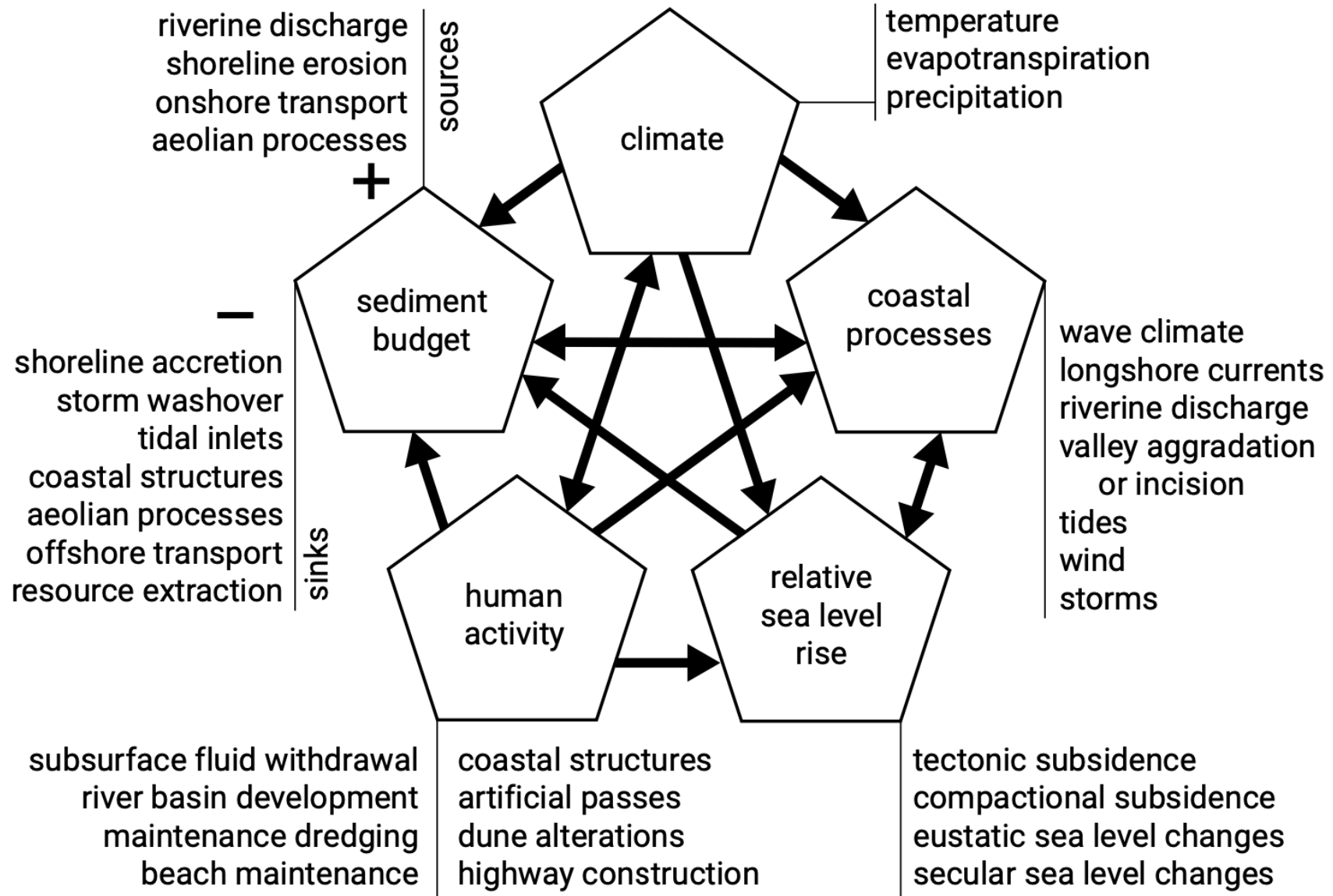


Figure 2.26: Interaction of agents affecting shore retreat and erosion according to Morton (1977).

CERC equation (Coastal Engineering Research Center)

To evaluate the sediment transported longshore, knowing the breaking wave height and the direction of wave attack, we can use

$$Q = 0,023 g^{1/2} * H^{5/2} * \sin 2\alpha (s^{-1})$$

where g is the acceleration of gravity and

$s = [(\rho_s)/(\rho)] - 1$ with ρ_s density of the transported sediment.

In this expression is not considered the direction and intensity of the stream and the dimension of the sediment.

The CERC formula gives the bulk longshore sediment transport – the total longshore sediment transport over the breaker zone – due to the action of waves approaching the coast at an angle.

Hence, only the effect of the wave-generated longshore currents is included; tidal currents or other alongshore currents are **not considered**.

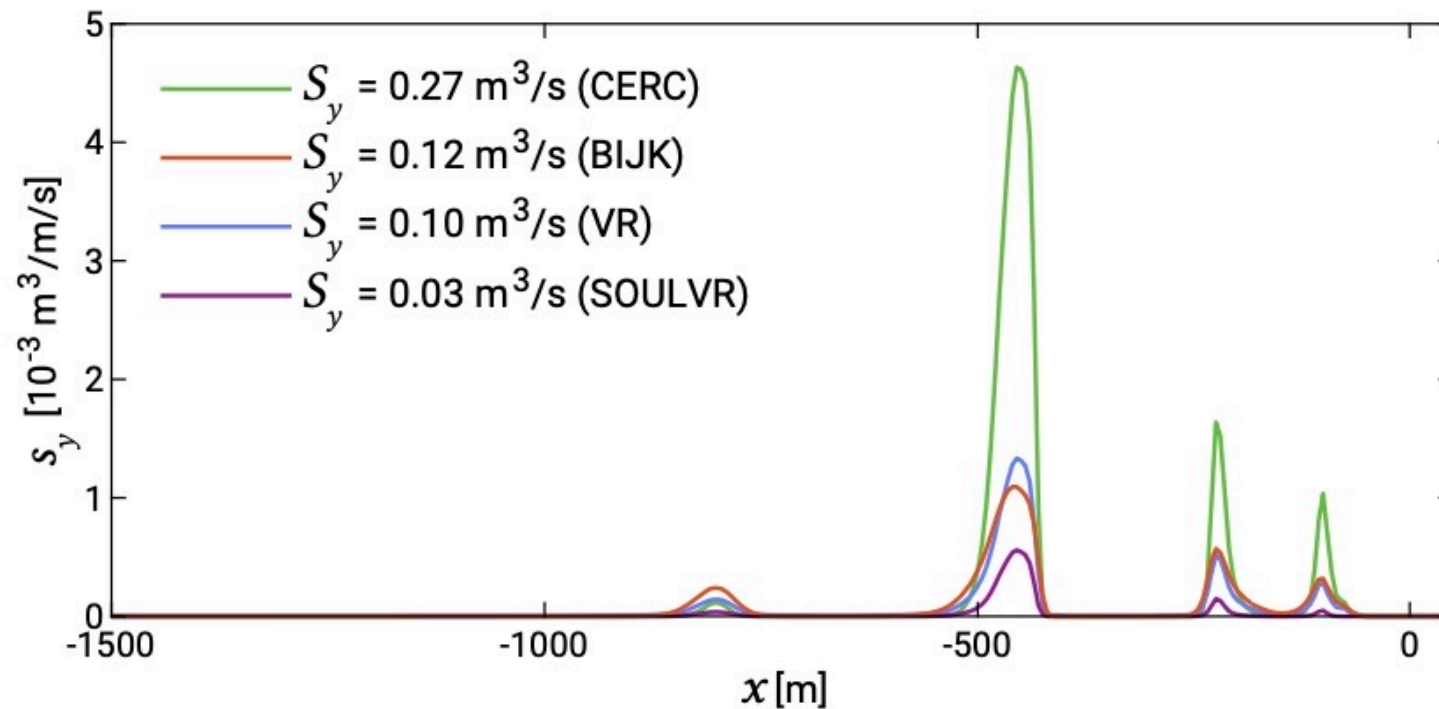
If the long- shore current is exclusively driven by waves, one can imagine that both the sediment concentration and longshore current velocity can be related in some way to the incident wave conditions.

$$S = \frac{I}{\rho g(s-1)(1-p)} = \frac{K}{\rho g(s-1)(1-p)} (Enc)_b \cos \varphi_b \sin \varphi_b \quad (8.4)$$

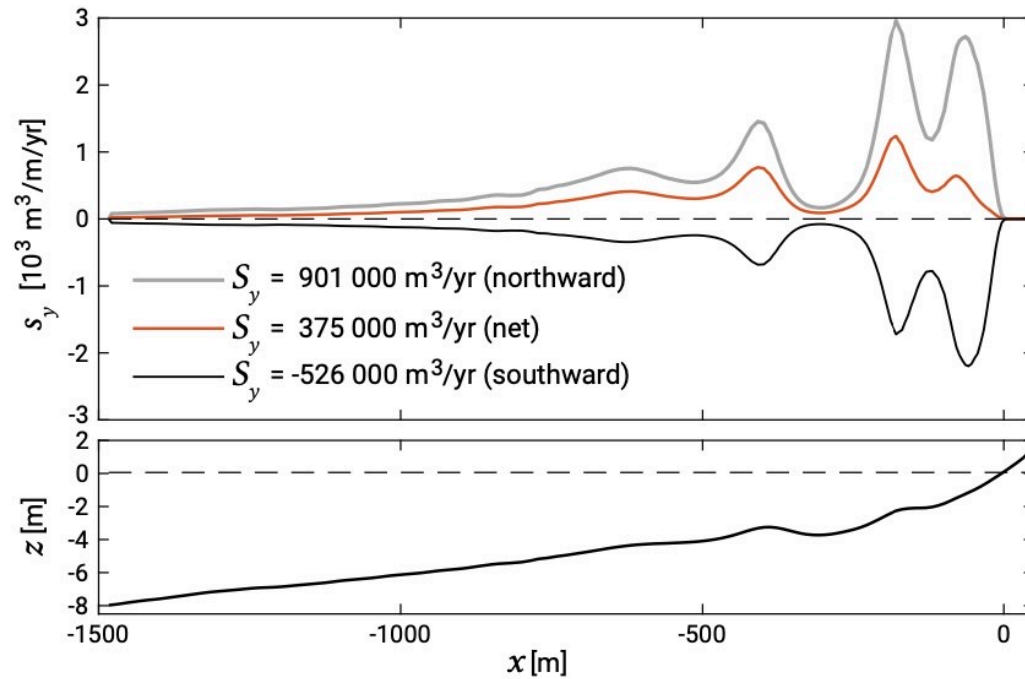
I	the immersed (underwater) weight of sediment transported, cf. Eq. 6.17	N/s
S	the deposited volume of sediment transported	m ³ /s
ρ	density of the water	kg/m ³
s	the relative density of the sediment ρ_s/ρ	–
p	porosity	–
g	gravitational acceleration	m/s ²
K	coefficient	–
E	wave energy	J/m ²
c	the wave phase velocity	m/s
n	the ratio between group and phase velocity	–
φ	the wave angle of incidence	–
b	subscript referring to conditions determined at the outer edge of the breaker zone	–

1. Only the wave-induced longshore current is taken into account; all other along- shore current driving forces, such as tidal currents, are ignored. In order to take the latter into account, more general transport formulas need to be applied.
2. The sand transport is independent of sand properties such as grain size. Also, the beach slope and hence the type of breakers is ignored (although the breaker index may be assumed to be dependent on the breaker type).
3. Only the total sediment transport in the breaker zone is given. It is often of practical importance to know how this transport is distributed over the width of the breaker zone, for instance if bars are present in the coastal profile, or if coastal structures are considered that do not entirely cover the breaker zone (such as groynes). However, this distribution could be estimated from a distribution for the longshore current velocity and wave-stirring capacity.

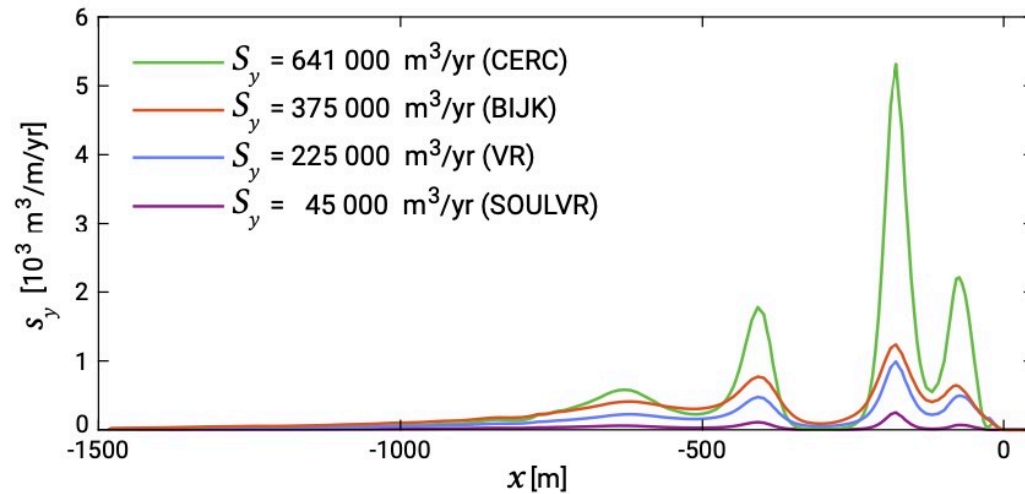
Longshore transport and coastline changes transport by assuming that the transport is proportional to the third power of the longshore current velocity $V(x)^3$. This procedure is followed for the CERC transport in the following figures



(b) sediment transport rates (deposited volumes) for $H_s = 2 \text{ m}$ and $T_p = 7 \text{ s}$ using four different transport formulas (CERC, Bijker (BIJK), Van Rijn (VR) and Soulsby Van Rijn (SOULVR)) with default settings (uncalibrated)



(a) net transport rates $s_y(x)$ and S_y (integrated over the cross-shore) using the Bijker transport formula and separated into gross (northward and southward) components



(b) net transport rates $s_y(x)$ and S_y (integrated over the cross-shore) using the transport formulas according to CERC, Bijker (BIJK), Van Rijn (VR) and Soulsby Van Rijn (SOULVR) without calibration (i.e. default settings are used)

It is important to identify the role of geographical information in participatory research of coastal zones, and its potential to bridge the gap between research and coastal zone management.

The GIS (Geographic Information System) produced temporal snapshots of daily human activity patterns allowing it to map, identify and quantify potential space-time conflicts between activities.

It was furthermore used to facilitate the exchange of ideas and knowledge at various levels: by mapping, simulation, GIS analysis and data collection.

The communication between science and society constitutes a relevant tool to optimize any planning and management project.

Dynamic GIS to illustrate different scenarios.

Table 1. Environmental Vulnerability Indexes (levels High, Medium, and Low) for the geoenvironmental units described on estuarines regions of Rio Grande do Norte State, as defined by GEOPRO (2002) from specific data.

<i>Geoenvironment Unit</i>	<i>Kind of Substratum</i>	<i>Mobility</i>	<i>Traffictility</i>	<i>Density of Biota</i>	<i>Indice of Environmental Vulnerability</i>
Tidal Plain	Fine Sand, Silt, and Clay	Low	Very Low	High	Medium
Mangroves	Fine Sand, Silt, and Clay	Low	Very Low	High Biodiversity	High
Plain of River Estuarine Flooding	Fine and Medium Sand	High	Low	High	Medium
Fixed Dunes/Interdune	Medium and Coarse Sand	Medium	Low	Low	Medium
Mobile Dunes/Interdune	Fine and Medium Sand	High	Low	Low	Medium
Planing Surface	Medium and Coarse Sand	Medium	High	Low	Low

Source: Souto et al., Journal of Coastal Research, ISSN 0749-0208

The SCAPE (Soft Cliff and Platform Erosion) model of cliff toe retreat, and a cliff-top recession model, have been linked with a new flexible GIS tool (SCAPEGIS) to provide visualisation and analytical capability for the model results. 45 model runs exploring different sealevel rise and wave climate scenarios and protection choices are available.

Outputs are available in the form of maps, dynamic visualisation, and descriptive statistics of key parameters such as cliff toe and cliff top position.

It also allows analysis with other datasets such as land use and building location for impact evaluation, and hence supports shoreline management and cliff-top land use planning.

Table 1. Summary defining the 45 scenarios used in the analysis in terms of relative sea-level rise, wave conditions (indicated by H_s low, etc.) and management approach.

Management Scenario (% of cliffed coast protected)	Relative sea-level rise scenario (2000 to 2100)								
	Low (0.2-m rise)				Mid (0.45-m rise)	High (1.2-m rise)			
	H_s low (no change)	H_s high (+10%)	H_s high + (+10% & +10°)	H_s high - (+10% & -10°)	H_s mid(+7%)	H_s low (no change)	H_s high (+10%)	H_s high + (+10% & +10°)	H_s high - (+10% & -10°)
1 (100%)	1	2	3	4	5	6	7	8	9
2 (71%)	10	11	12	13	14	15	16	17	18
3 (34%)	19	20	21	22	23	24	25	26	27
4 (16%)	28	29	30	31	32	33	34	35	36
5 (0%)	37	38	39	40	41	42	43	44	45

1. Beach additions (yearly totals): The average amount of sediment added to the beach from platform and cliff erosion at each Y section each year
2. Beach volume (yearly average): The average volume of sediment along 500-m sectors of coast held in beaches at each Y section each year.
3. Recession distances: The total amount of cliff toe recession at each Y section each year.
4. Longshore sediment flux moving past the southern and northern boundaries of the cliffed section every tide. The annual net sediment flux can be calculated by adding the first 703 tides together (703 tides per year).
5. The average relative level of the shore platform near the cliff toe for each Y section every year.

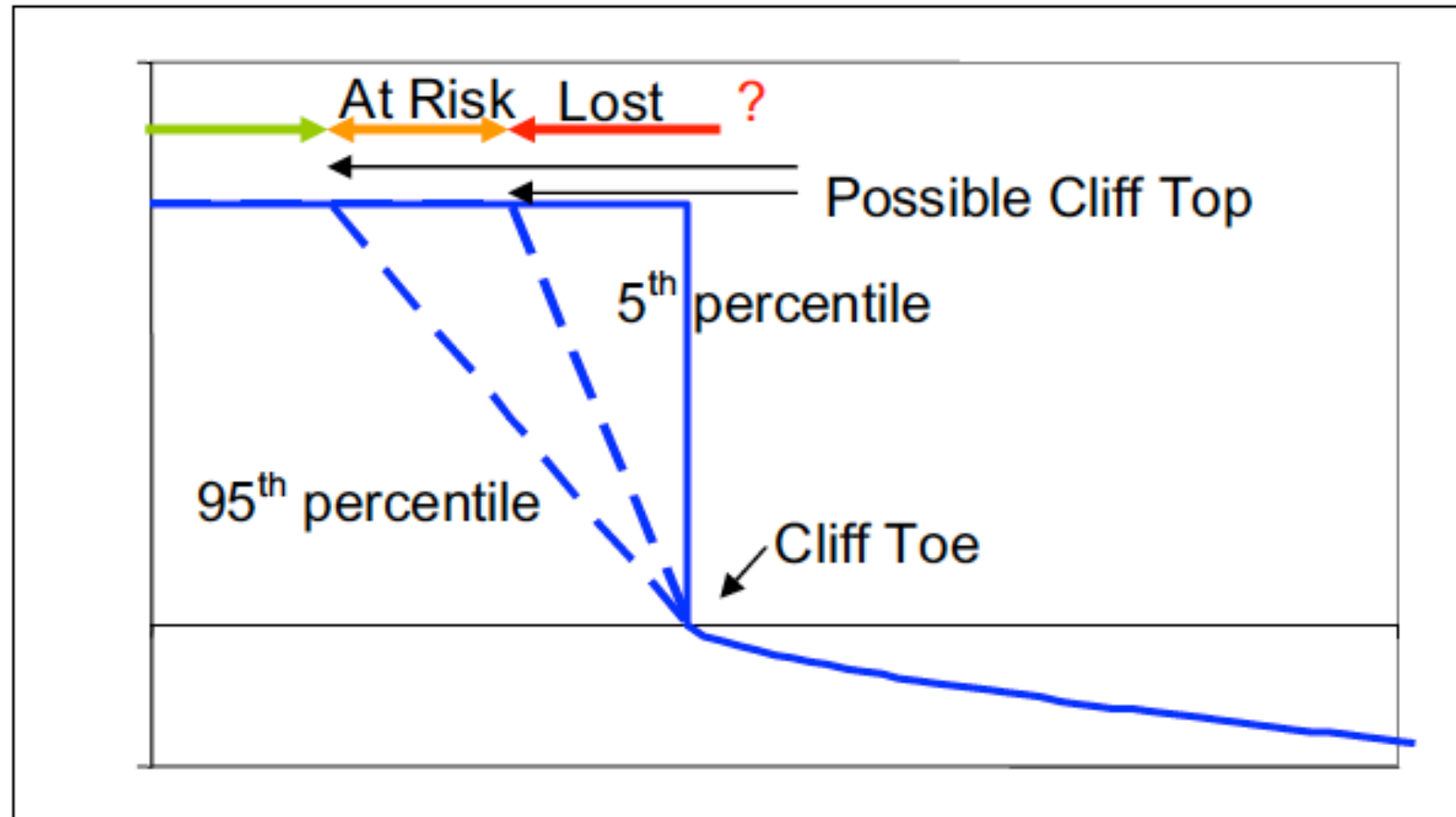


Fig. 4. Areas lost and at risk on the cliff-top. All other areas are considered safe



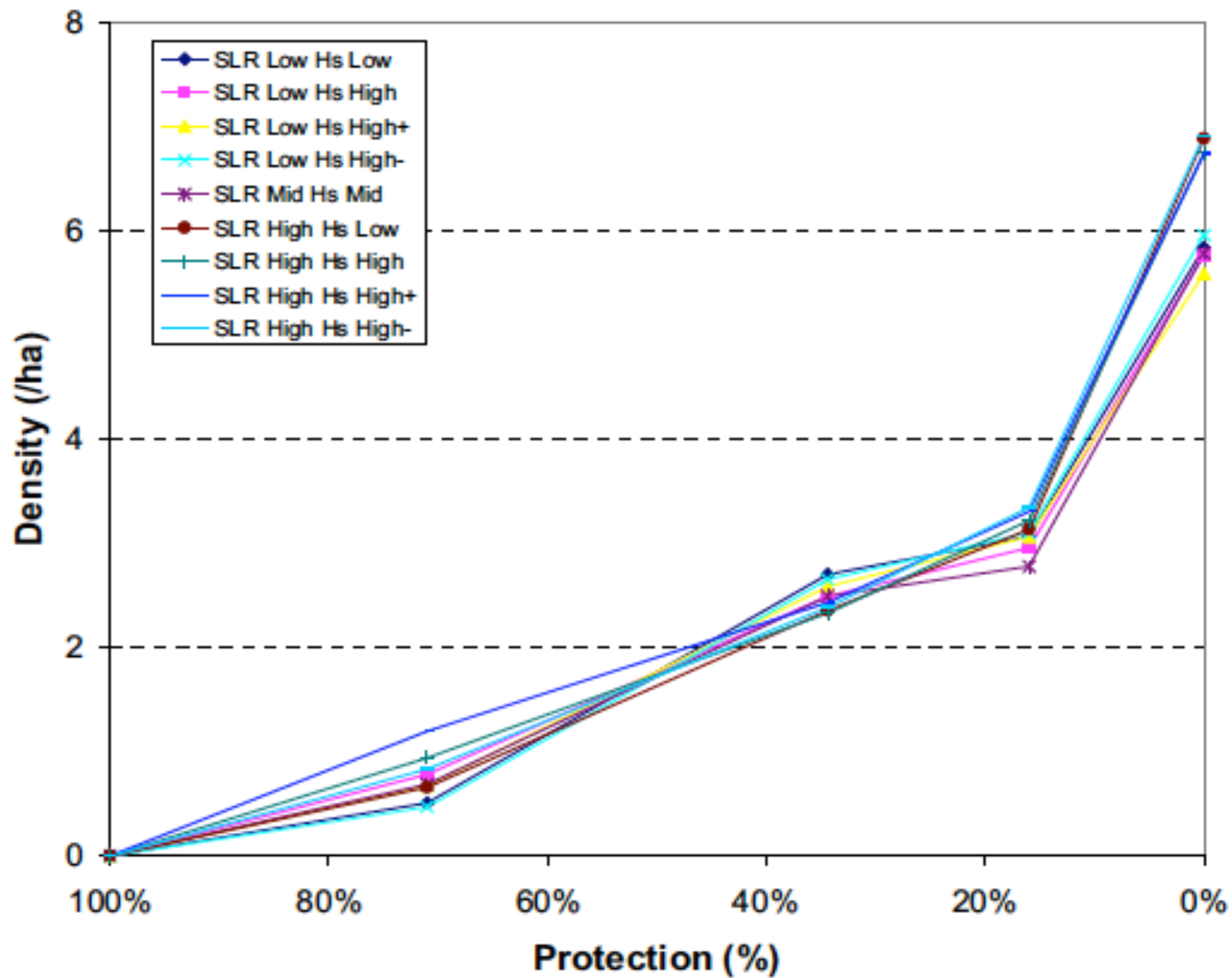
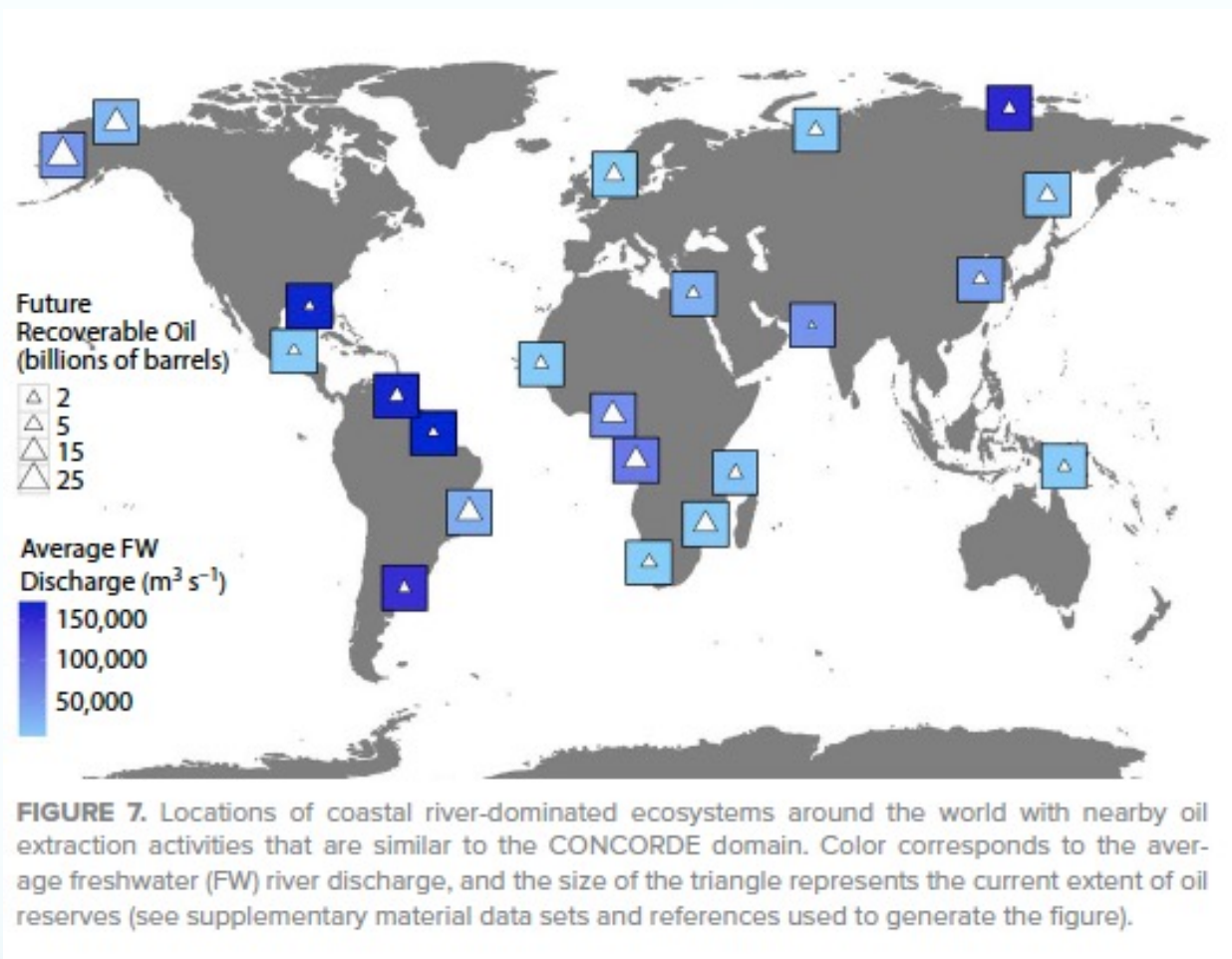


Fig 8. Residential property density on areas subject to land loss, versus the amount of protection. Results are shown for a range of climate scenarios.



Source: <https://doi.org/10.5670/oceanog.2018.302>

Table 1

List of the most significant port area accidents in terms of the quantity of hazardous substances involved

AN	Year	Location	Description	Operation	Quantity (tonnes)	Substance
316	1976	Spain; A Coruña	Tanker "Urquiola"; release of crude oil into sea	Approach	100,000	Crude oil
1132	1979	Turkey; Istanbul	Massive fire + explosions at port after collision between ships; killed 52 people	Manoeuvre	95,000	Crude oil
2787	1975	Portugal; Leixoes	Accident caused by Danish tanker "Jacob Maersk"	Manoeuvre	89,999	Crude oil
4575	1989	Morocco; Khark 5	Release of crude oil	Manoeuvre	70,000	Crude oil
1515	1981	Italy; Genoa	Tanker "Hakuyoh Maru" struck by lightning	Loading/unloading	58,999	Crude oil
171	1976	Ecuador; Guayaquil	Explosion on jetty after a short circuit on unloading tanker ignited LNG vapours	Loading/unloading	50,001	LNG
871	1979	Germany; Duisburg	Explosion affecting 17 port tanks + release into water	Storage	34,000	Oil
6698	1993	Indonesia; Sumatra	Collision between tankers "Sanko Honour" and "Maersk Navigator"	Manoeuvre	32,000	Crude oil
1196	1980	Turkey; Istanbul; Karadeniz Bogazi	Collision of Greek ship "Stawanda" with British "Nordic Faith"	Approach	28,299	Kerosene
4132	1990	Portugal; Madeira	Crude oil spilled from tanker reached coast of Madeira and Porto Santo	Approach	25,000	Crude oil

AN = MHIDAS accident no.

Source: Ronza et al ,2003, Journal of Loss Prevention in the Process Industries 16, 551-560.

Table 2
List of the most significant accidents that have occurred after 1970 in terms of the number of casualties

AN	Year	Location	Description	Operation	Killed	Injured	Substances
8721	1997	India; Andhra Pradesh, Visakhapatnam	Huge fire spread during unloading of a ship	Loading/unloading	56	20	Crude oil; kerosene; LPG; petroleum products
1132	1979	Turkey; Istanbul	Massive fire + explosions at port after collision between ships: killed 52 people	Manoeuvre	52	3	Crude oil
1851	1975	USA; Pennsylvania; Marcus Hook	Collision between tankers	Manoeuvre	26	35	Crude oil
5882	1992	Malaysia; Strait of Malacca	Collision between tanker and container vessel	Manoeuvre	22		Crude oil
2851	1987	Philippines; Manila	Fire spread from a tanker unloading into two barges	Loading/unloading	15		Methyl methacrylate
6946	1994	Iran; Bandar Khomeini	Explosion + fire at wheat silo in port	Storage	13	26	Wheat
5618	1992	Malaysia; Port Kelang	Explosion + huge fire on chemical tanker at depot	Loading/unloading	13		Toluene; xylene
2783	1987	Italy; Porto San Vitale	Explosion/fire during maintenance work on LPG carrier "Elisabetta Montanari"	Maintenance	13		LPG
2677	1974	USA; Pennsylvania; Fort Mifflin	Tanker "Elias" wrecked by series of explosions while berthed	Loading/unloading	13	8	Crude oil
893	1979	USA; Louisiana; Good Hope	Collision of cargo vessel with loading butane barge; fireball lasting 1 min	Manoeuvre	12		Butane

AN = MHIDAS accident no.

Table 5

Classification of the accidents in terms of the type of operation

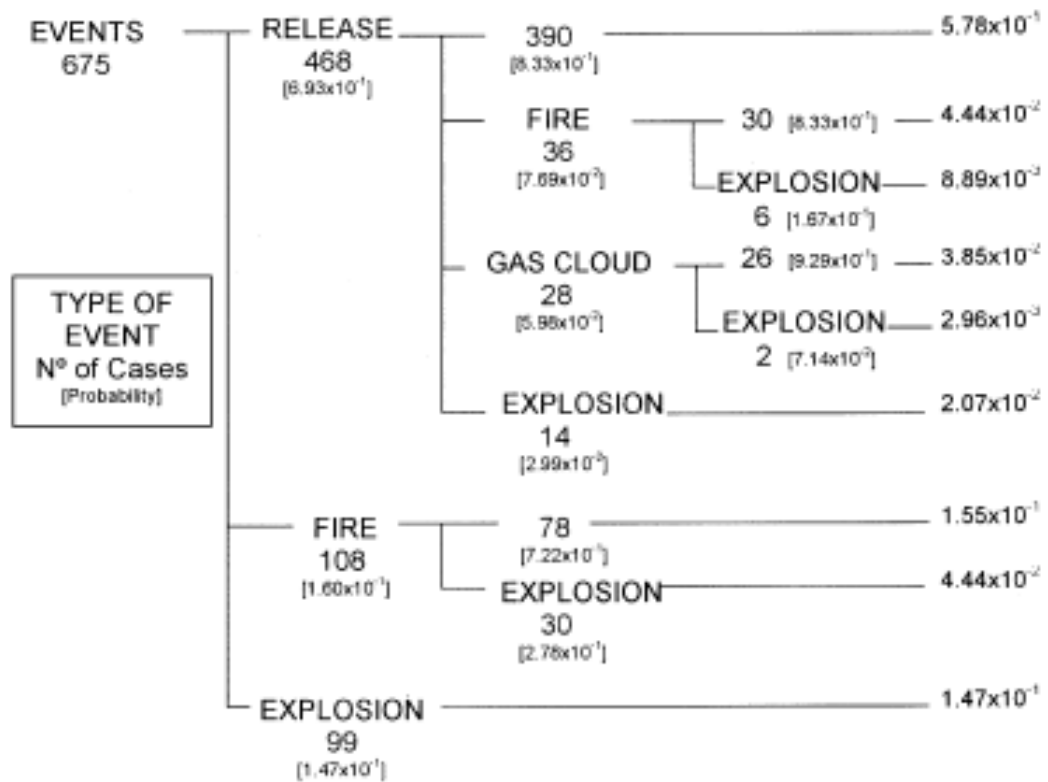
Operation	Number of accidents	%
Loading/unloading	280	34
Manoeuvre	224	27
Approach	108	13
Storage	101	12
Transport	56	7
Maintenance	40	5
Process	19	2
Total	828	100

Table 6
Elements that caused the accident

Element	Number of accidents	(%)
Warehouse	100	12.1
Pipeworks	77	9.3
Hose	38	4.6
Valve	20	2.4
Drum	20	2.4
Lorry	12	1.4
Rail tanker	7	0.8
Crane	2	0.2

Table 7
Ranking of the substances most frequently involved

Substance	Number of accidents	(%)
Crude oil	148	17.9
Fuel oil	59	7.1
Oil	47	5.7
Gasoline	45	5.4
Chemicals	25	3.0
Ammonia	22	2.7
Gas oil	21	2.5
Diesel fuel	21	2.5
Petrol	20	2.4
LPG	19	2.3



- <https://www.riskaware.co.uk/insight/oil-spill-impact-on-marine-environment/>

<https://www.marineinsight.com/environment/15-major-oil-spills-of-the-maritime-world/>

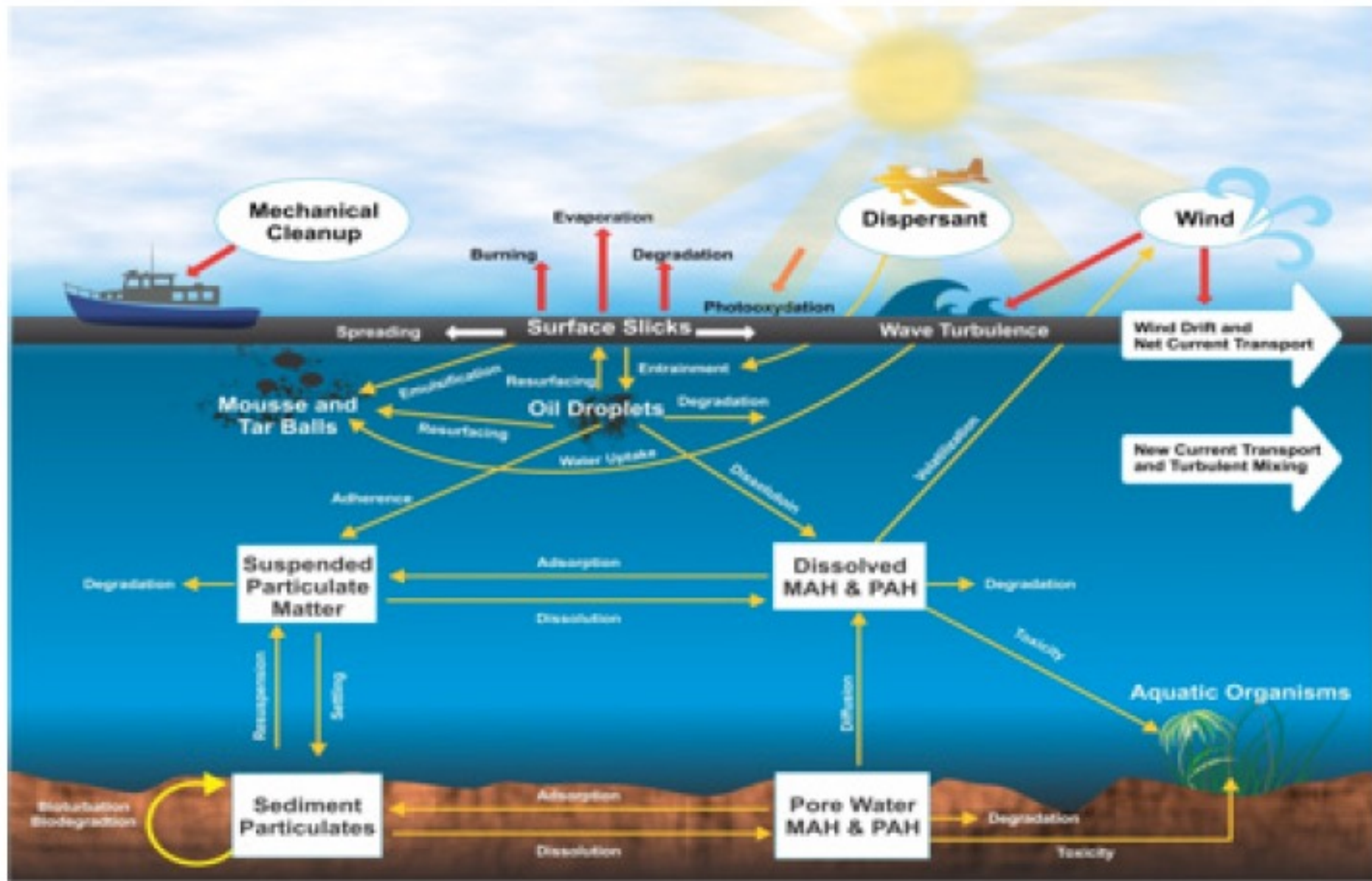


Arctic

Modeling Oil Spills in the Beaufort Sea

Exploring the Risk: What would happen if oil spills in the Beaufort Sea?





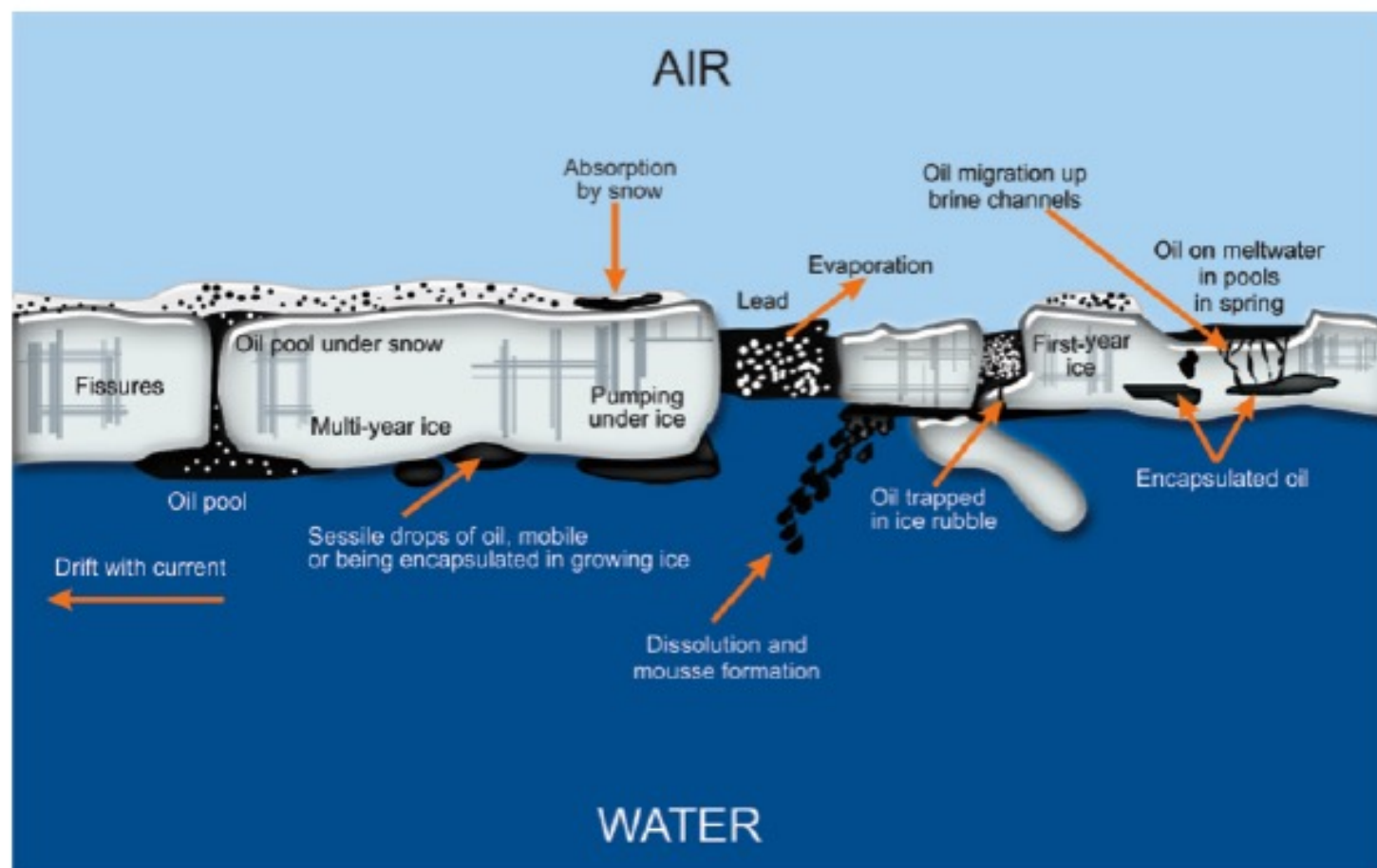


Figure 4. General schematic showing dynamics and characteristics of sea ice and oil interaction at the sea surface.
 (Source: Original figure by Alan A. Allen).

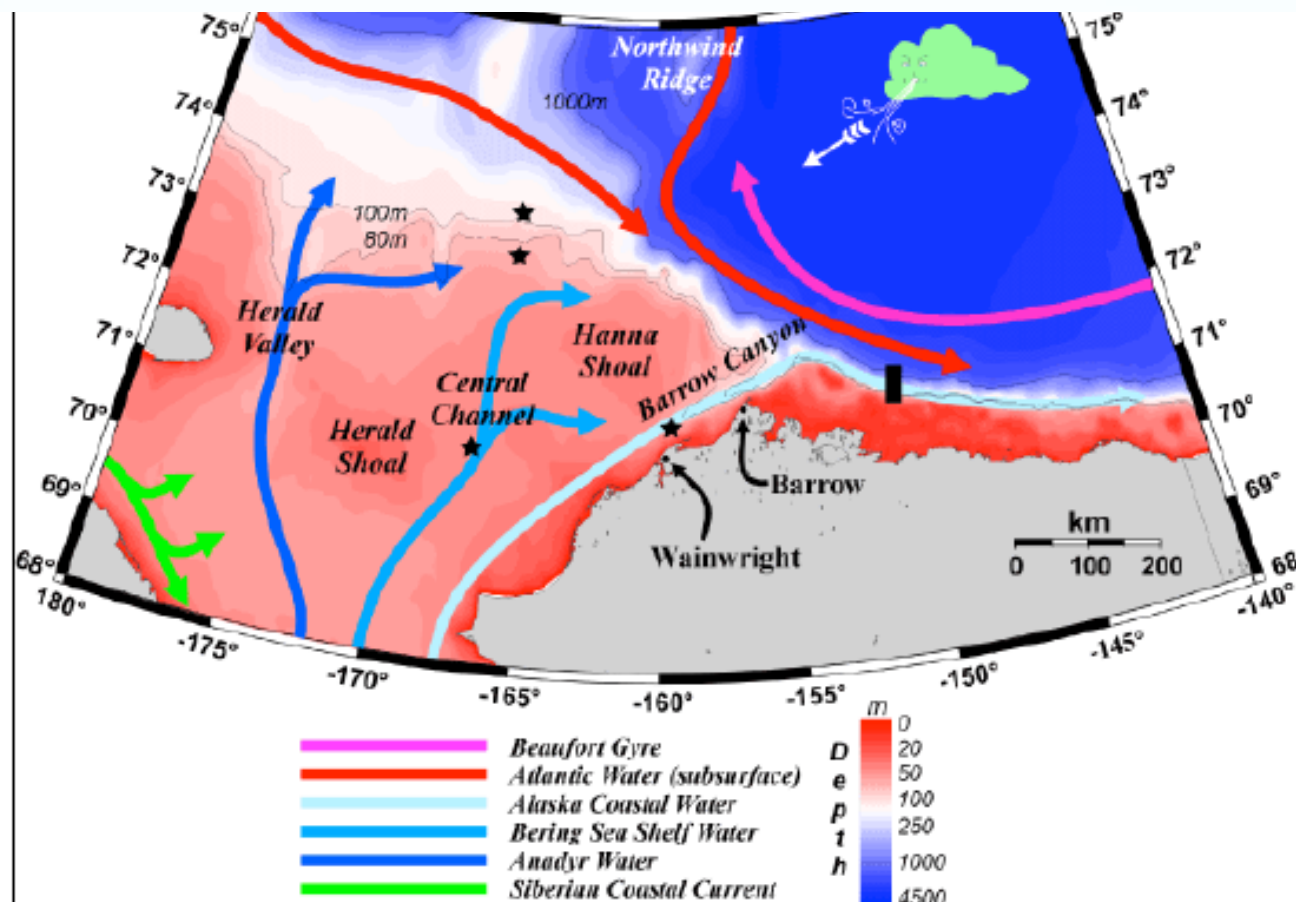


Figure 8. Main currents in Chukchi and Beaufort Seas. The three inflowing Pacific branches are color-coded with navy blue being the most nutrient rich waters and light blue being the least nutrient rich. The Siberian Coastal

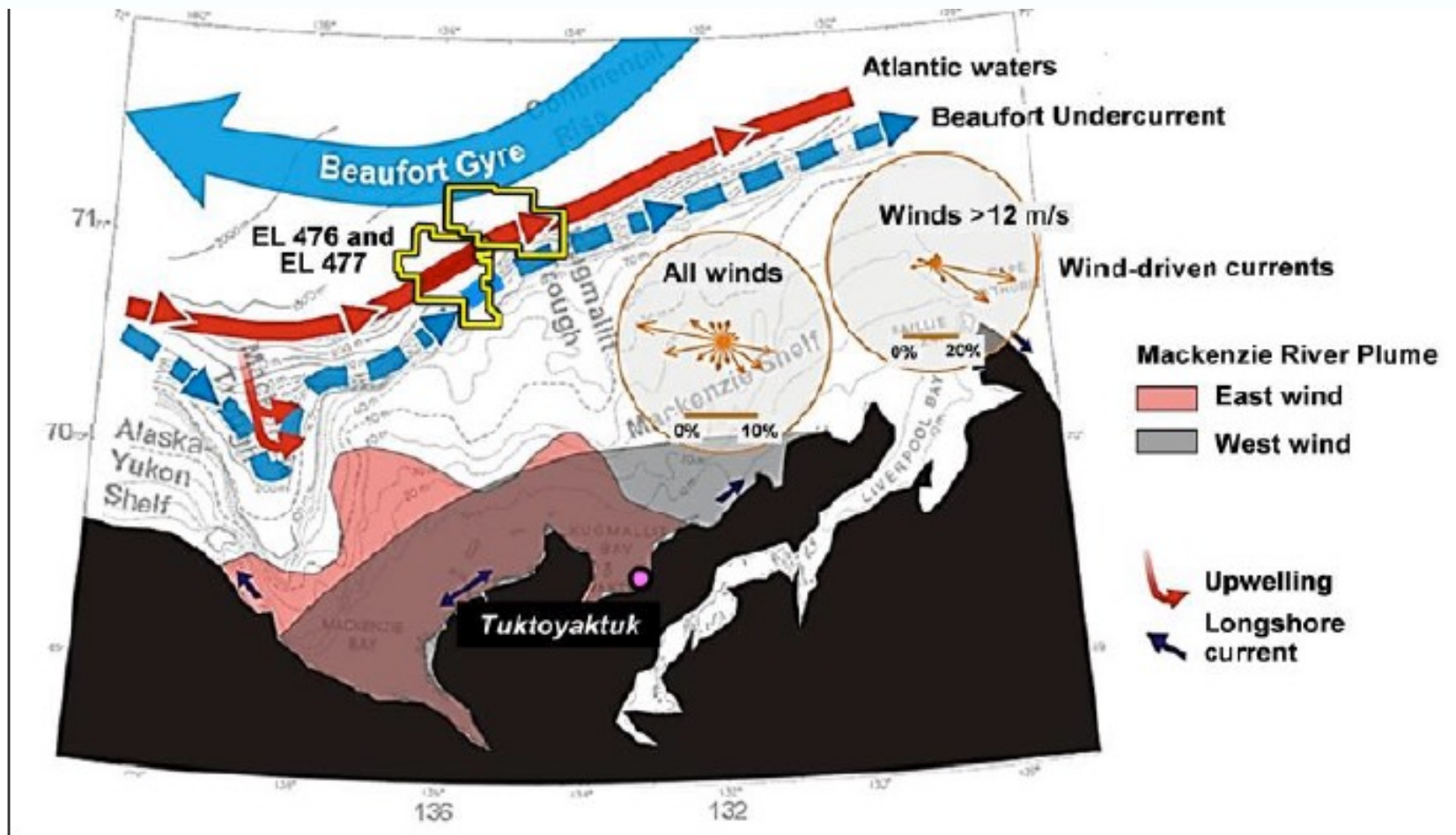
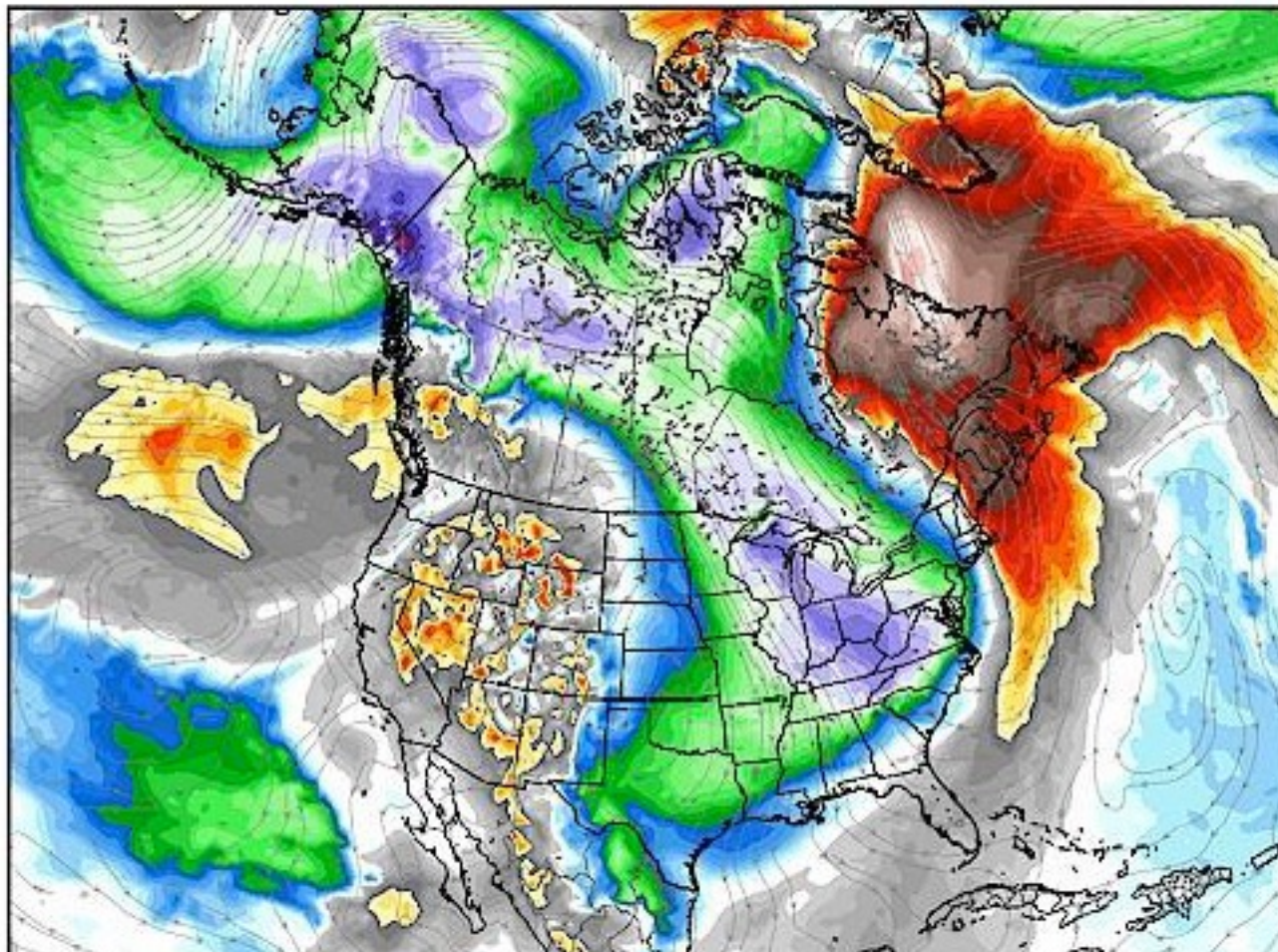


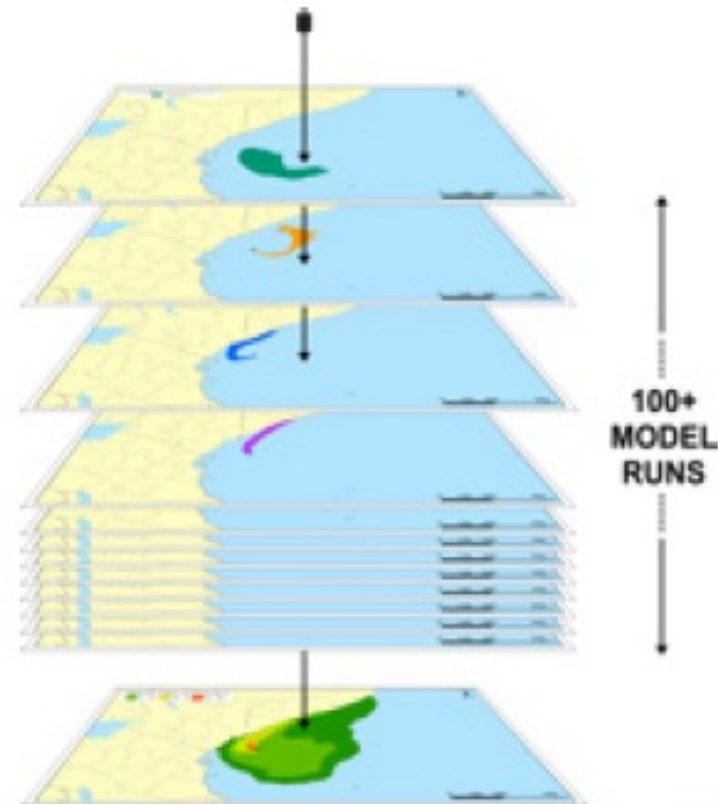
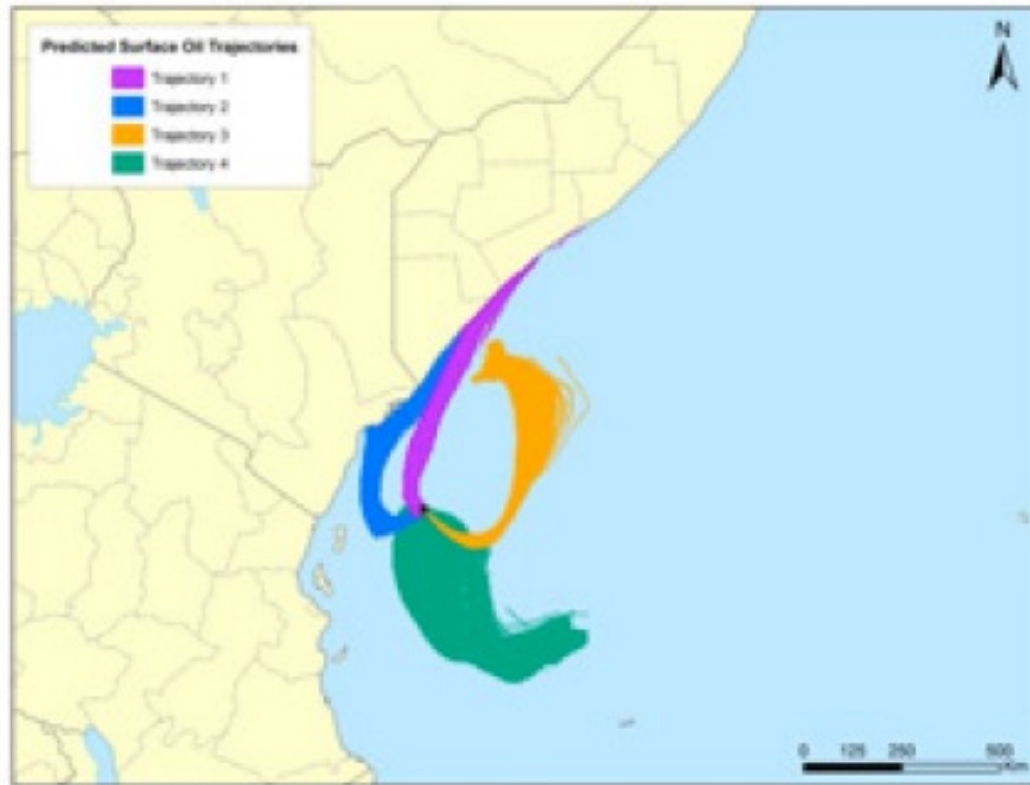
Figure 10. Ocean currents and winds in the Canadian Beaufort Sea (Source: COVU, 2013)

2. Modelled shore widths and oil holding capacities for each shore type (French et al., 1996).

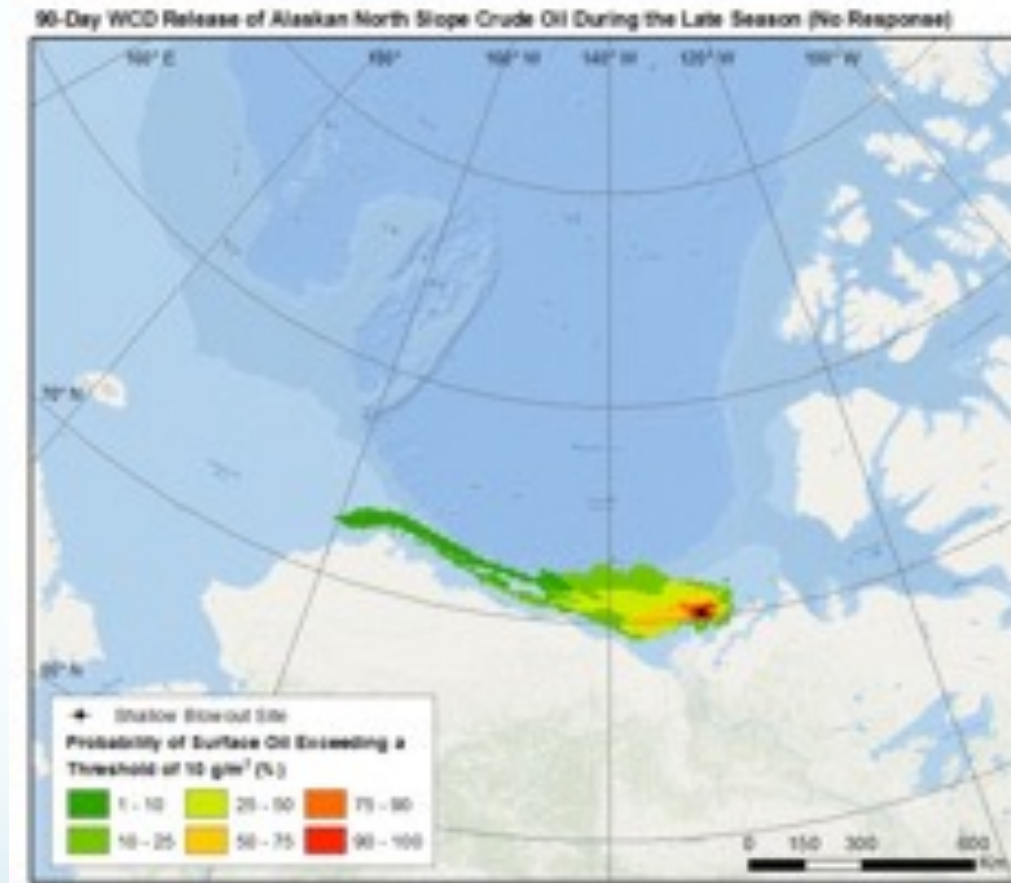
Type of Shore	Width (m)	Oil Holding Capacity (mm)		
		Oil Viscosity < 30 cSt	Oil Viscosity 30 – 2,000 cSt	Oil Viscosity > 2,000 cSt
Rocky Shore	2	1.0	2.0	2.0
Gravel Beach	3	2.0	9.0	15.0
Sand Beach	10	4.0	17.0	25.0
Mud Flat (Seaward)	10	3.0	6.0	10.0
Mud Flat (Landward)	140	6.0	30.0	40.0
Wetland (Saltmarsh)	140	6.0	30.0	40.0
Intertidal Macroalgal	2	1.0	2.0	2.0
Artificial Shore	0.1	0.01	0.1	0.1

EC

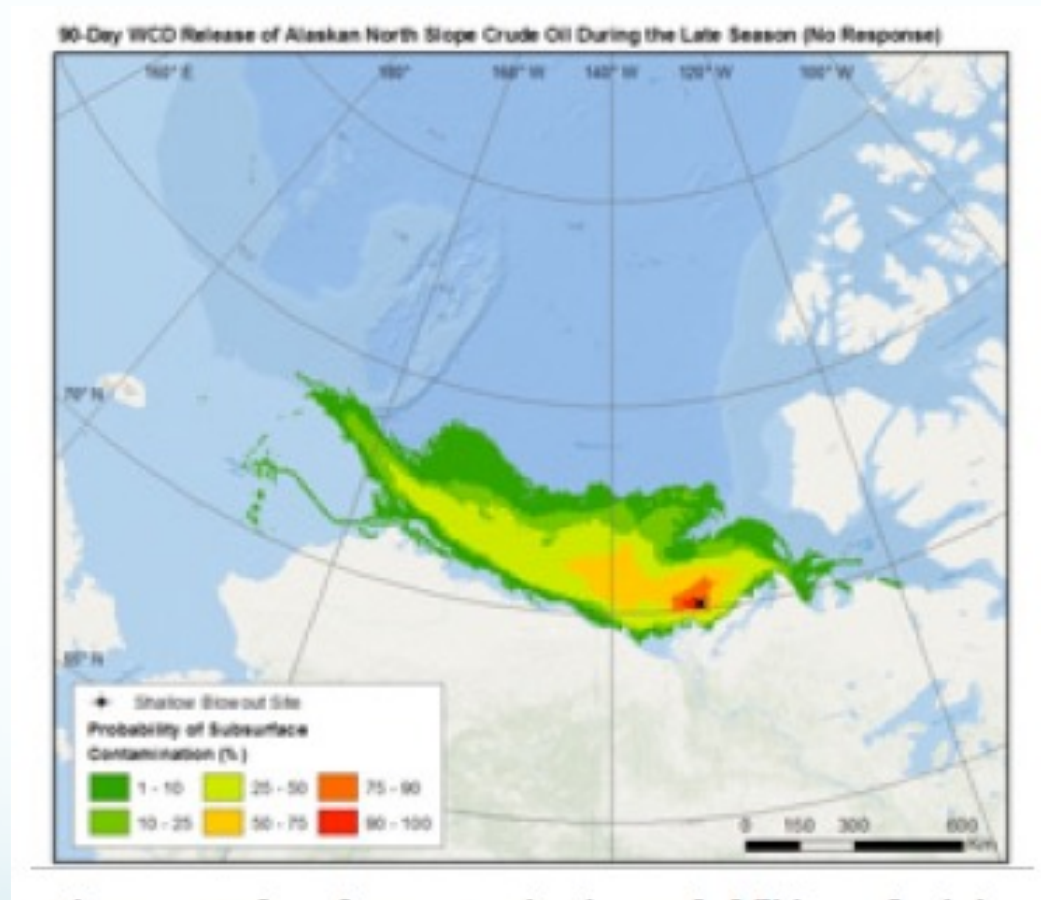




Examples of four individual spill trajectories predicted by SIMAP (*Spill Impact Modeling Application*) for a generic spill scenario. All 100+ individual trajectories are overlain (shown as the stacked runs on the right), and the frequency of contact with given locations is used to calculate the probability of how oil can affect an area during a spill. (Source: Gearon et al., 2014)



Water surface oiling probabilities for floating oil $> 10 \text{ g/m}^2$
(source Geraon et al., 2014)



Subsurface contamination probabilities for total oil in the water column (Source Gearon et al, 2014)